

Supporting information for

# Plasmonic-Magnetic Active Nanorheology for Intracellular Viscosity

*Sungwoo Lee<sup>a,b,†</sup>, Insub Jung<sup>a,b,†</sup>, Soohyun Lee<sup>a</sup>, Junghyun Shin<sup>c</sup>, Eunbyeol Cha<sup>o</sup>, Sangbaek Jung<sup>a</sup>,  
Seongkeun Ih<sup>a</sup>, Yang-Gyun Kim<sup>a</sup>, Seunghun Hong<sup>c</sup>, Yoon-La Choi<sup>d,e</sup>, and Sungho Park<sup>a,\*</sup>*

<sup>a</sup>Department of Chemistry, Sungkyunkwan University (SKKU), Suwon, 16419, Republic of  
Korea

<sup>b</sup>Institute of Basic Science, Sungkyunkwan University (SKKU), Suwon, 16419, Republic of  
Korea

<sup>c</sup>Department of Physics and Astronomy, Institute of Applied Physics, Seoul National University  
(SNU), Seoul, 08826, Republic of Korea

<sup>d</sup>Department of Health Sciences and Technology, SAIHST, Sungkyunkwan University  
(SKKU), Seoul, 06355, Republic of Korea

<sup>e</sup>Department of Pathology and Translational Genomics, Samsung Medical Center,  
Sungkyunkwan University School of Medicine, Seoul, 06351, Republic of Korea

Keywords: Plasmonic, Magnetic, Nanorheology, Viscosity, Cancer cells

\*e-mail: spark72@skku.edu

†: These authors contributed equally

## **Table of contents**

<b>Experimental section .....</b>	<b>8</b>
<b>Figure S1. Schematic illustration on synthesis of Au/Ni/Au nanorods. ....</b>	<b>15</b>
<b>Figure S2. Low-magnification FE-SEM images of Au/Ni/Au NRs. (A-B) .....</b>	<b>16</b>
<b>Figure S3. A field-emission scanning electron microscopy (FE-SEM) image, energy dispersive spectroscopy (EDS) elemental mapping images, and EDS spectrum of Au/Ni/Au nanorods.....</b>	<b>17</b>
<b>Figure S4. FE-SEM images and their physical dimensions of Au/Ni/Au nanorods with varying length of Au and Ni segments for stability test. ....</b>	<b>18</b>
<b>Figure S5. Stability test of Au/Ni/Au nanorods with varying length of Au segment and Ni segment.....</b>	<b>19</b>
<b>Figure S6. Stability test of Au/Ni/Au NRs with varying lengths of Au segments and Ni segments shown in panel A in Fig. 2.....</b>	<b>20</b>
<b>Figure S7. Aggregated NRs do not provide FTSPR signals.....</b>	<b>21</b>
<b>Supplementary Note 1. Measurement of viscosity of glycerol solution using commercial viscometers.....</b>	<b>22</b>
<b>Figure S8. Raw FTSPR data for viscosity measurement of water (viscosity = <math>1.02 (\pm 0.01)</math> cP). .....</b>	<b>24</b>
<b>Figure S9. Raw FTSPR data for viscosity measurement of 41% glycerol solution (viscosity = <math>5.01 (\pm 0.05)</math> cP). ....</b>	<b>25</b>

<b>Figure S10. Raw FTSPR data for viscosity measurement of 55% glycerol solution (viscosity = 10.32 (<math>\pm 0.02</math>) cP).</b>	<b>26</b>
<b>Figure S11. Raw FTSPR data for viscosity measurement of 61% glycerol solution (viscosity = 15.37 (<math>\pm 0.01</math>) cP).</b>	<b>27</b>
<b>Figure S12. Raw FTSPR data for viscosity measurement of 66% glycerol solution (viscosity = 21.01 (<math>\pm 0.01</math>) cP). (A-C) Raw optical response data and (D-F) their corresponding frequency peak data after FFT. Optical response data were obtained under driving frequencies from 15 rpm to 550 rpm at a measurement wavelength of 570 nm.</b>	<b>28</b>
<b>Figure S13. Raw FTSPR data for viscosity measurement of 70% glycerol solution (viscosity = 25.3 (<math>\pm 0.1</math>) cP).</b>	<b>29</b>
<b>Figure S14. Raw FTSPR data for viscosity measurement of 72% glycerol solution (viscosity = 31.3 (<math>\pm 0.1</math>) cP).</b>	<b>30</b>
<b>Figure S15. Raw FTSPR data for viscosity measurement of 74% glycerol solution (viscosity = 35.3 (<math>\pm 0.1</math>) cP).</b>	<b>31</b>
<b>Figure S16. Optimization of monitoring wavelength for Fourier transform surface plasmon resonance (FTSPR) of Au/Ni/Au nanorods.</b>	<b>32</b>
<b>Figure S17. A FE-SEM image of single-component Au nanorods, and their corresponding vis-NIR spectra dispersed in 0% (water) and 75% glycerol solution.</b>	<b>33</b>
<b>Supplementary Note 2. The estimation of the concentration of Au/Ni/Au nanorods</b>	<b>34</b>
<b>Figure S18. FEM simulation for the dynamics of Au/Ni/Au NRs (dimension: diameter = 74 nm, 174-145-174 nm) under the condition of without and with surrounding medium with</b>	

different viscosities (1, 10, 20, 30 and 40 cP) and driving frequencies (from 0.25 to 8.33 Hz).

.....35

**Supplementary Note 3. Critical frequency of Au/Ni/Au nanorods with different configuration of component .....36**

**Figure S19. Physical dimensions of Au-Ni-Au nanorods for theoretical simulation. ....36**

**Figure S20. FEM simulation for the dynamics of Au/Ni/Au NRs (dimension: diameter = 74 nm, 50-393-50 nm) under the condition of without and with surrounding medium of different viscosities (1, 10, 20, 30 and 40 cP) and driving frequencies (from 0.25 to 8.33 Hz).....37**

**Figure S21. FEM simulation for the dynamics of Au/Ni/Au NRs (dimension: diameter = 74 nm, 96-301-96 nm) under the condition of without and with surrounding medium of different viscosities (1, 10, 20, 30 and 40 cP) and driving frequencies (from 0.25 to 8.33 Hz).....38**

**Figure S22. FEM simulation for the dynamics of Au/Ni/Au NRs (dimension: diameter = 74 nm, 211-71-211 nm) under the condition of without and with surrounding medium of different viscosities (1, 10, 20, 30 and 40 cP) and driving frequencies (from 0.25 to 8.33 Hz).  
.....39**

**Figure S23. FEM simulation for the dynamics of Au/Ni/Au NRs (dimension: diameter = 74 nm, 231-31-231 nm) under the condition of without and with surrounding medium with different viscosities (1, 10, 20, 30 and 40 cP) and driving frequencies (from 0.25 to 8.33 Hz).  
.....40**

**Figure S24. Angular displacement of Au/Ni/Au NRs with different physical dimensions at a fixed time point (0.2 sec) as a function of driving frequency for different solution viscosities.  
.....41**



<b>Figure S25. Zeta potential data and FE-SEM images of Au/Ni/Au nanorods before and after surface modification with MUTAB. ....</b>	<b>42</b>
<b>Figure S26. MTT assay results for cell cytotoxicity of Au/Ni/Au nanorods in HeLa, Hep G2, MCF-7, and HUF cells. ....</b>	<b>43</b>
<b>Figure S27. X-ray photoelectron spectroscopy (XPS) analysis of Au/Ni/Au nanorods...44</b>	
<b>Figure S28. Localization of Au/Ni/Au NRs in living cells. ....</b>	<b>45</b>
<b>Figure S29. Raw FTSPR data for viscosity measurement of HeLa cells (measurement 1, 2, and 3). ....</b>	<b>46</b>
<b>Figure S30. Raw FTSPR data for viscosity measurement of HeLa cells (measurement 4, 5, and 6). ....</b>	<b>47</b>
<b>Figure S31. Raw FTSPR data for viscosity measurement of HeLa cells (measurement 7, 8, and 9). ....</b>	<b>48</b>
<b>Figure S32. Raw FTSPR data for viscosity measurement of HeLa cells (measurement 10). ....</b>	<b>49</b>
<b>Figure S33. Raw FTSPR data for viscosity measurement of Hep G2 cells (measurement 1, 2, and 3). ....</b>	<b>50</b>
<b>Figure S34. Raw FTSPR data for viscosity measurement of Hep G2 cells (measurement 4, 5, and 6). ....</b>	<b>51</b>
<b>Figure S35. Raw FTSPR data for viscosity measurement of Hep G2 cells (measurement 7, 8, and 9). ....</b>	<b>52</b>

<b>Figure S36. Raw FTSPR data for viscosity measurement of Hep G2 cells (measurement 10).</b>	
.....	<b>53</b>
<b>Figure S37. Raw FTSPR data for viscosity measurement of MCF-7 cells (measurement 1, 2, and 3).</b>	
.....	<b>54</b>
<b>Figure S38. Raw FTSPR data for viscosity measurement of MCF-7 cells (measurement 4, 5, and 6).</b>	
.....	<b>55</b>
<b>Figure S39. Raw FTSPR data for viscosity measurement of MCF-7 cells (measurement 7, 8, and 9).</b>	
.....	<b>56</b>
<b>Figure S40. Raw FTSPR data for viscosity measurement of MCF-7 cells (measurement 10).</b>	
.....	<b>57</b>
<b>Figure S41. Raw FTSPR data for viscosity measurement of HUF cells (measurement 1, 2, and 3).</b>	
.....	<b>58</b>
<b>Figure S42. Raw FTSPR data for viscosity measurement of HUF cells (measurement 4, 5, and 6).</b>	
.....	<b>59</b>
<b>Figure S43. Raw FTSPR data for viscosity measurement of HUF cells (measurement 7, 8, and 9).</b>	
.....	<b>60</b>
<b>Figure S44. Raw FTSPR data for viscosity measurement of HUF cells (measurement 10).</b>	
.....	<b>61</b>
<b>Figure S45. Vis-NIR spectrum and CLSM image of Au/Ni/Au nanorods taken up by HeLa cells.</b>	
.....	<b>62</b>

<b>Figure S46. Raw FTSPR data for viscosity measurement of cell culture medium and buffer solution.....</b>	<b>63</b>
<b>Figure S47. Raw FTSPR data for viscosity measurement of HeLa, Hep G2, MCF-7, and HUF cells obtained immediately after adding Au/Ni/Au nanorods in the cell solution.....</b>	<b>64</b>
<b>Table S1. A comparison table of intracellular viscosity measurement .....</b>	<b>65</b>
<b>References .....</b>	<b>66</b>

## Experimental section

### Instrumentation

Scanning electron microscopy (FE-SEM) images of nanoparticles were obtained using field-emission scanning electron microscopy (JSM-7100, JSM-7800F, JEOL). Transmission electron microscopy (TEM) images of nanoparticles were obtained using high-resolution transmission electron microscopy (JEM-ARM 200F, JEOL). Visible and near-infrared (vis-NIR) spectra were obtained using a vis-NIR spectrophotometer (UV-3600, Shimadzu). We conducted simulations through finite-element methods (FEM) (COMSOL Multiphysics, 5.0 ver.). Zeta potentials of nanoparticles were obtained using a dynamic light scattering (DLS) instrument (Zetasizer NanoZs90, Malvern). X-ray photoelectron spectra were obtained using X-ray photoelectron spectroscopy (ESCALAB 250Xi, Thermo scientific). Immunofluorescence analysis was conducted with confocal laser scanning microscopy (TCS SP8 Hyvolution, Leica Microsystems CMS GmbH).

### Synthesis of Au/Ni/Au nanorods

We synthesized Au/Ni/Au nanorods through a hard template-assisted potentiostatic electrochemical deposition method following our previous protocol.<sup>1-3</sup> We fabricated anodized aluminum oxide (AAO) templates for synthesis of Au/Ni/Au nanorods by following the method in previously published literature.<sup>1</sup> For electrochemical deposition of nanorods, a thin sacrificial layer of Ag was coated on the one side of the AAO template using an Ar plasma sputter-coater (Cressington 108 auto) with a current level of 30 mA for 600 s, which serves as a working electrode

in the three-electrode electrochemical system after making physical contact with a conductive Al foil electrode in the Teflon cell. Electrochemical deposition was performed on a potentiostat/galvanostat (AutoLab, PGSTAT12). A Ag/AgCl electrode and Pt mesh were utilized as the reference electrode and the counter electrode, respectively. First, a commercially available Ag plating solution (1025 RTU, Technic Inc.) was reduced on the conducting Ag layer cathode at the bottom at -0.95 V (vs. Ag/AgCl). The Au, Ni, and Au layers were electroplated on the surface using commercially available Au plating solution (Orotemp 24 RTU, Technic Inc.) and Ni plating solution (nickel(II) sulfate hexahydrate,  $\text{NiSO}_4 \cdot 6\text{H}_2\text{O}$ , 10 g/ 100 mL, 98.5%, Daejung; boric acid,  $\text{H}_3\text{BO}_3$ , 3 g/ 100 mL, 99.5%, Duksan), respectively, at -0.95 V (vs. Ag/AgCl). We controlled the lengths of the nanorods by monitoring the total charge that passed through the cell.

Then, Ag was selectively etched with 60% nitric acid ( $\text{HNO}_3$ , 60.0%, Samchun). After synthesis of nanorods in the AAO template, the AAO template was dissolved in 3 M sodium hydroxide ( $\text{NaOH}$ , 98.0%, Samchun) to release the synthesized nanorods. The released nanorods were rinsed several times with triply distilled water to remove residual ions. The nanorods were dispersed in ethanol and sonicated to disperse nanorods. Then, nanorods in ethanol were dried in an oven to fully remove ethanol. Nanorods were redispersed in  $\text{D}_2\text{O}$  solvent for optical property characterization, and a small number of nanorods were drop-casted onto a silicon oxide wafer to obtain FE-SEM images.

#### *Surface modification of Au/Ni/Au nanorods with (11-mercaptoundecyl)-N,N,N-trimethylammonium bromide (MUTAB)*

We modified the surface of Au/Ni/Au nanorods with MUTAB (in ethanol) as follows. After

releasing Au/Ni/Au nanorods from a piece of AAO template, we rinsed nanorods with triply distilled water to remove residual ions. The nanorods were dispersed in ethanol, sonicated to disperse nanorods and dried in an oven. Then, we added 0.1 mL of 0.2 mM (11-mercaptoundecyl)-N,N,N-trimethylammonium bromide (MUTAB, dissolved in ethanol, Sigma-Aldrich) for 1 h at room temperature. After surface modification, we centrifuged nanorods at 10,000 rpm for 5 min and washed with ethanol twice. After removal of ethanol, we dispersed MUTAB modified Au/Ni/Au nanorods in triply distilled water for further experiments.

#### *Fourier transform surface plasmon resonance (FTSPR) experimental setups*

We conducted Fourier transform surface plasmon resonance (FTSPR) experiments with Au/Ni/Au nanorods by following the methods reported in previously published literatures.<sup>4-6</sup> A magnetic stirrer (dimensions: 11 cm × 12 cm × 2 cm, field strength: 1 mT, Neuatation) was placed under a cuvette containing Au/Ni/Au nanorods in the solution to apply an external magnetic field to the Au/Ni/Au nanorods. Throughout the experiment, the total volume of analytes was fixed at 0.1 mL. While applying an external rotating magnetic field with a magnetic stirrer, we monitored the extinction intensity of Au/Ni/Au nanorods for 6.325 s at an interval of 25 ms by irradiating incoming light through a vis-NIR spectrophotometer (Scinco, S-3100). To obtain a peak at the frequency domain, we converted extinction intensity values obtained from Au/Ni/Au nanorods to frequency domain spectra using fast Fourier transform (FFT). It is to note that only FTSPR peaks with a signal to noise ratio over 4 were considered. For the measurement of viscosity of glycerol solution, we first added Au/Ni/Au nanorods in an Eppendorf tube and fully dried the surrounding Au/Ni/Au nanorods in an oven. Then, we added a glycerol solution with varying water and glycerol

volume fractions to the Eppendorf tube containing Au/Ni/Au nanorods. The glycerol solution was made by mixing glycerol (99.5%, Sigma-Aldrich) and water. After mixing Au/Ni/Au nanorods with glycerol solution, we conducted a FTSPR experiment to measure viscosity.

### *Cell culture*

HeLa (ATCC<sup>®</sup> CCL-2<sup>™</sup>, ATCC) cells and Hep G2 (ATCC<sup>®</sup> HB-8065<sup>™</sup>, ATCC) were cultured in Eagle's minimum essential medium (EMEM, Catalog No. 30-2003, ATCC) supplemented with 10% fetal bovine serum (FBS, Gibco) and 1% penicillin-streptomycin-amphotericin B (PCS-999-002, ATCC) in a 37°C, 5% CO<sub>2</sub> environment and grown until ~80 % confluent.

MCF7 (ATCC<sup>®</sup> HTB-22<sup>™</sup>, ATCC) cells were cultured in Eagle's minimum essential medium (EMEM, Catalog No. 30-2003, ATCC) supplemented with 10% fetal bovine serum (FBS, Gibco), 1% penicillin-streptomycin-amphotericin B (PCS-999-002, ATCC), and 0.01 mg/mL insulin (human recombinant, Sigma-Aldrich) in a 37°C, 5% CO<sub>2</sub> environment and grown until ~80 % confluent.

Primary uterine fibroblast cells (Normal, Human, HUF, ATCC<sup>®</sup> PCS-460-010<sup>™</sup>, ATCC) cells were cultured in fibroblast basal medium (FBM, ATCC PCS-201-030, ATCC) supplemented with Fibroblast Growth Kit-Low Serum (ATCC PCS-201-041, containing L-glutamine, hydrocortisone hemisuccinate, rh FGF  $\beta$ , rh insulin, ascorbic acid, and fetal bovine serum, ATCC) and 1% penicillin-streptomycin-amphotericin B (PCS-999-002, ATCC) in a 37°C, 5% CO<sub>2</sub> environment and grown until ~80 % confluent. Cells at passages 20-30 were used for whole experiment.

### *MTT assay*

We incubated cells (5,000 cells/well) in 96-well plates in a 37°C, 5% CO<sub>2</sub> environment. After 24 h of incubation, we added MUTAB modified Au/Ni/Au nanorods dispersed in phosphate buffered saline (1X PBS, 21-040-CV, set a final concentration of Au/Ni/Au nanorods as 5 pM in each well, Corning) and incubated the solution for another 6 h in a 37°C, 5% CO<sub>2</sub> environment. We removed cell culture medium and residual Au/Ni/Au nanorods in the wells, and added MTT solution (20 µL, 5 mg/mL in PBS, Sigma-Aldrich). Cells were incubated with a MTT solution in a 37°C, 5% CO<sub>2</sub> environment for 5 h to generate formazan crystals. After removing the MTT solution, we added 100 µL of DMSO (≥99.5%, Sigma-Aldrich) to quantify the amount of formazan crystals using a microplate reader (Varioskan LUX, thermoscientific) measured at 560 nm.

### *Immunofluorescence analysis*

We labelled Au/Ni/Au nanorods with Rhodamine B dye as follows. We mixed 0.1 mL of 1 mg/mL Rhodamine B-PEG-thiol (RhB, dispersed in ethanol, molecular weight: 3400, Nanocs) with MUTAB modified Au/Ni/Au nanorods for 6 h in a 70°C oven. After labelling, we washed Au/Ni/Au nanorods with ethanol twice by centrifugation to remove residual free RhB in the solution. We incubated 5,000 cells with RhB labelled Au/Ni/Au nanorods on the cover slip in a 37°C, 5% CO<sub>2</sub> environment. After performing fixation of cells with 1 mL of 4% paraformaldehyde (Biosolution) for 15 min, cells were permeabilized with 0.3% Triton<sup>TM</sup> X-100 (Sigma-Aldrich). Then, HeLa, Hep G2, MCF-7, and HUF cells were incubated with rabbit anti-Human PDIA4 monoclonal antibody (1:60, Sino Biological), rabbit anti-Human FDPS monoclonal antibody (1:60, Sino Biological), rabbit anti-Human CDNP1 monoclonal antibody (1:60, Sino Biological), and



rabbit anti-Human Fibronectin Fragment 2 polyclonal antibody (1:1000, Sino Biological), respectively, for 6 hours in a 37°C, 5% CO<sub>2</sub> environment. After washing with PBS, cells were stained with Alexa Fluor® 488-conjugated goat anti-rabbit IgG secondary antibody (Invitrogen) and counterstained with DAPI (Invitrogen) for 15 min. After washing with PBS again, from CLSM images, the nucleus, cytoplasm, and Au/Ni/Au nanorods exhibited blue, green, and red fluorescence, respectively.

#### *TEM sample preparation for cell imaging*

We incubated cells and Au/Ni/Au nanorods on the confocal dish for TEM analysis. First, cells were fixed with 1 mL of Karnovsky's fixative solution (2% glutaraldehyde, 2% paraformaldehyde in 0.05 M sodium cacodylate buffer) and 1% osmium tetroxide solution (diluted in 0.1 M cacodylate buffer) for primary fixation and post fixation, respectively. After washing with water three times, we stained cells with 0.5% uranyl acetate (diluted in distilled water) overnight at 4°C. After cell fixation, we dehydrated cells with ethanol. Dehydrated cells were infiltrated in Spurr's resin for 48 h at 70°C for the resin polymerization. We cut samples with an ultramicrotome (EM UC7, Leica) and placed them on copper grids. We analyzed cell samples with a TEM (Talos L120C, FEI) at an acceleration voltage of 120 kV.

#### *The protocol of intracellular viscosity measurement using Au/Ni/Au nanorods and FTSPR setup*

We trypsinized HeLa, Hep G2, and MCF-7 cells on the cell culture dish with 1 mL of 0.25% trypsin-EDTA (1X) solution (Gibco) to detach cells for 5 min in a 37°C, 5% CO<sub>2</sub> environment.

After detaching cells from the cell culture plate, we transferred cells with trypsin EDTA to a conical tube and added 5 mL of cell complete growth media, which was then centrifuged to remove residual trypsin EDTA from cells at 800 rpm for 5 min.

We trypsinized HUF cells on the cell culture dish with 1 mL of trypsin-EDTA for primary cell (ATCC PCS-999-003, ATCC) detachment for 5 min in a 37°C, 5% CO<sub>2</sub> environment. After detaching cells from cell culture plate, we transferred cells with trypsin-EDTA for primary cells to a conical tube and added 5 mL of Dulbecco's phosphate buffered saline (D-PBS, 1X, ATCC) and 1 mL of trypsin neutralizing solution (ATCC PCS-999-004, ATCC), which was then centrifuged to remove residual trypsin EDTA from cells at 800 rpm for 5 min.

After centrifugation, supernatant containing cell culture medium and growth media was removed. Cells were dispersed in PBS. We estimated the number of cells using a hemocytometer. We prepared 5,000 cells/80 µL PBS by diluting cells with PBS. Then, we added 20 µL of MUTAB modified nanorods to make the final concentration of Au/Ni/Au nanorods 5 pM to analyze the intracellular viscosity of cells.

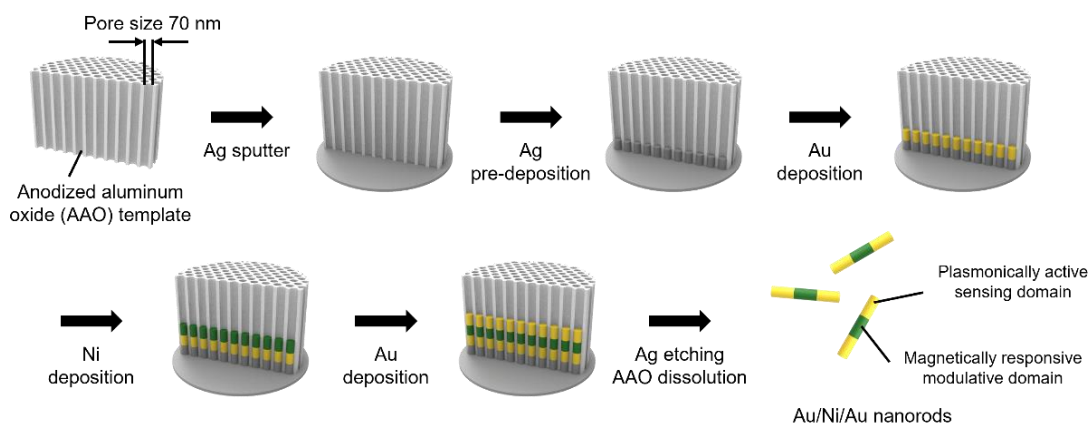


**Figure S1. Schematic illustration on synthesis of Au/Ni/Au nanorods.** Au/Ni/Au nanorods were synthesized through a template-mediated potentiostatic electrochemical deposition technique. A thin backing layer of Ag (working as a conducting layer) was coated on the one side of the AAO template by a sputter coater. In the Ag pre-deposition step, we reduced Ag by injecting Ag precursor solution on the conducting Ag layer cathode at a constant potential of -0.95 V (vs. Ag/AgCl). Then, Au, Ni, and Au were deposited consecutively at -0.95 V (vs. Ag/AgCl). For releasing Au/Ni/Au nanorods, Ag was selectively etched with 60% nitric acid followed by AAO dissolution using 3 M sodium hydroxide. Nanorods were rinsed with triply distilled water four times to remove residual ions.

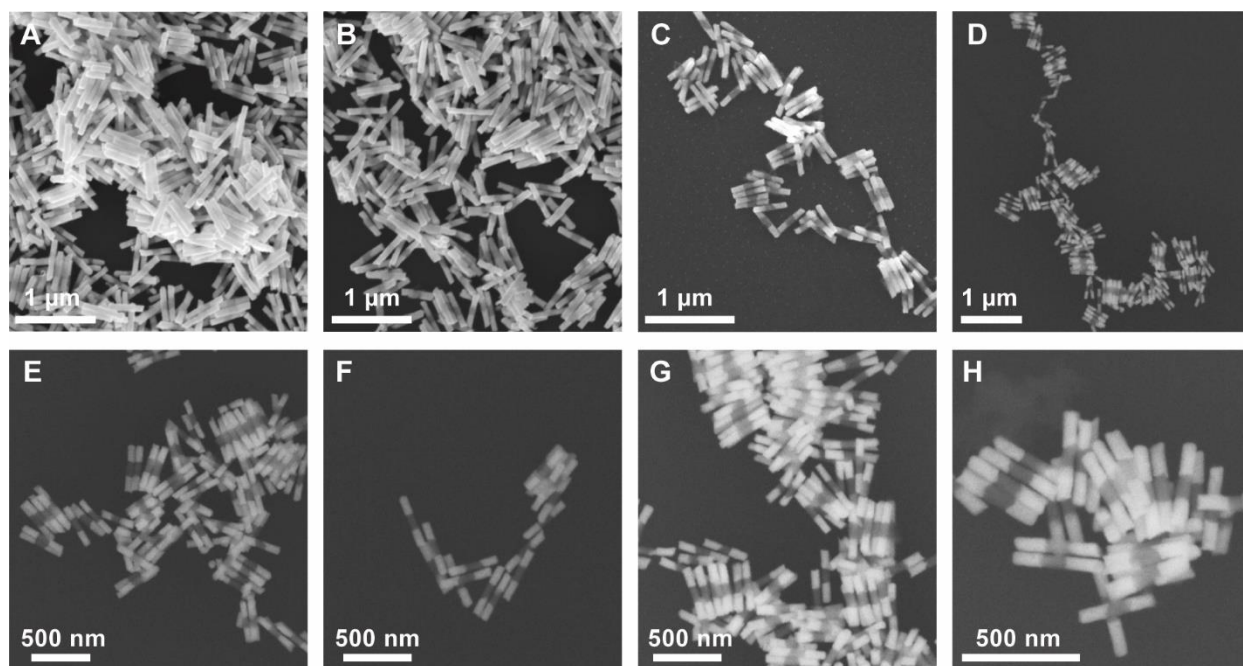


**Figure S2. Low-magnification FE-SEM images of Au/Ni/Au NRs. (A-B)** Bright FE-SEM images **(C-H)** backscattered electron mode of FE-SEM images of Au/Ni/Au NRs shown in Figure 2a.

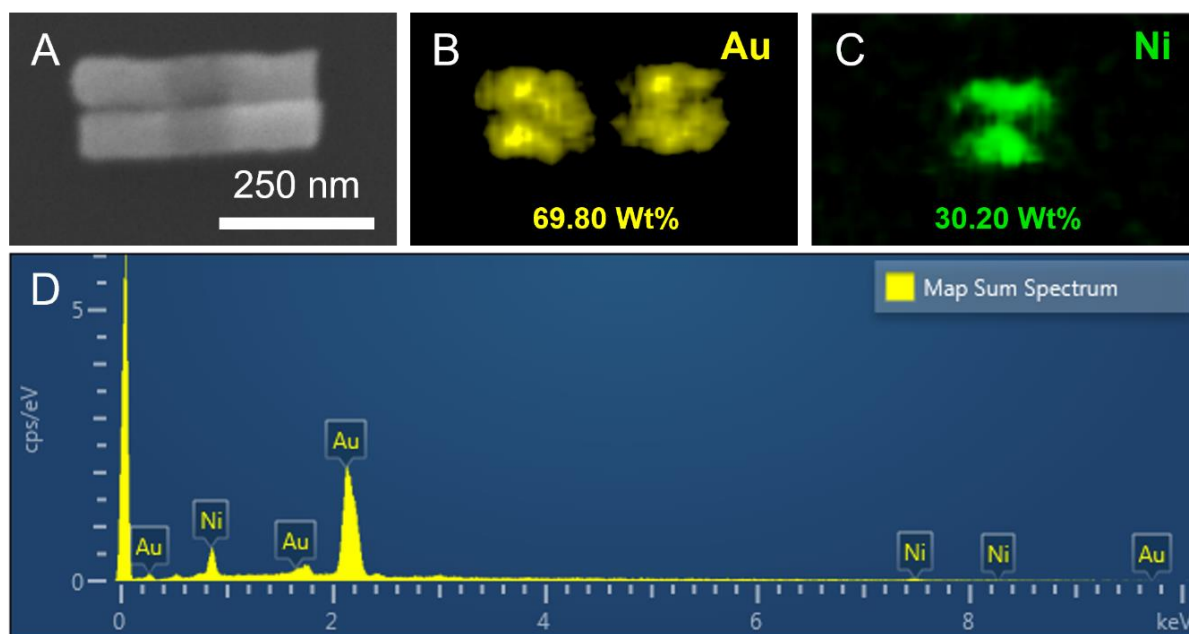


**Figure S3.** A field-emission scanning electron microscopy (FE-SEM) image, energy dispersive spectroscopy (EDS) elemental mapping images, and EDS spectrum of Au/Ni/Au nanorods. **(A)** A FE-SEM image of Au/Ni/Au nanorods. **(B-D)** We confirmed the existence of Au and Ni from Au/Ni/Au nanorods through EDS analysis.

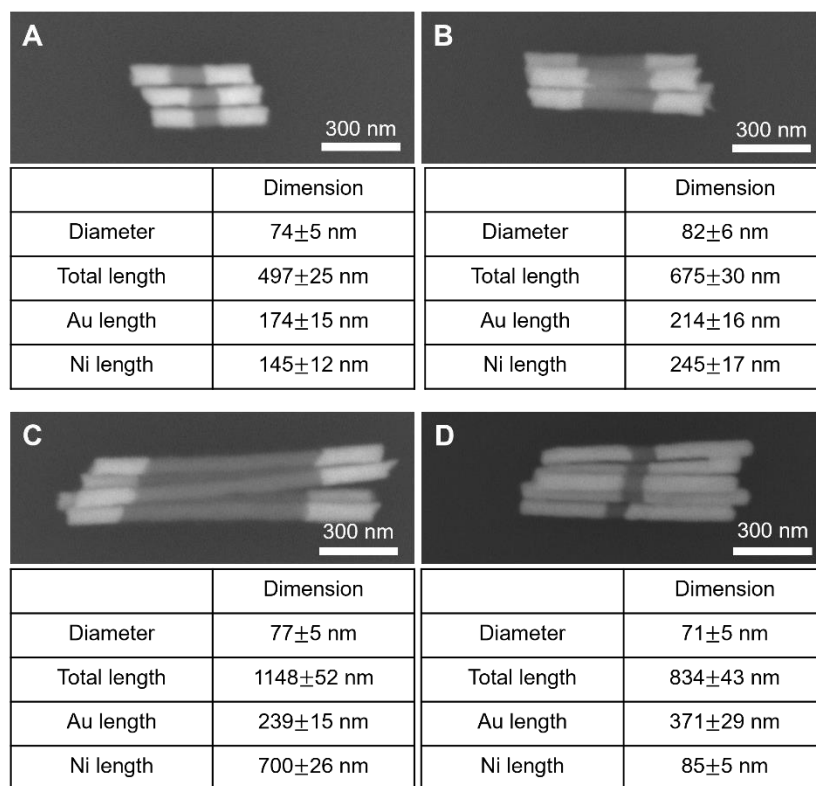


**Figure S4. FE-SEM images and their physical dimensions of Au/Ni/Au nanorods with varying length of Au and Ni segments for stability test. (A-D)** FE-SEM images of Au/Ni/Au nanorods utilized for stability test shown in Figure S5 and their physical dimensions (diameter, total length, Au length, and Ni length).

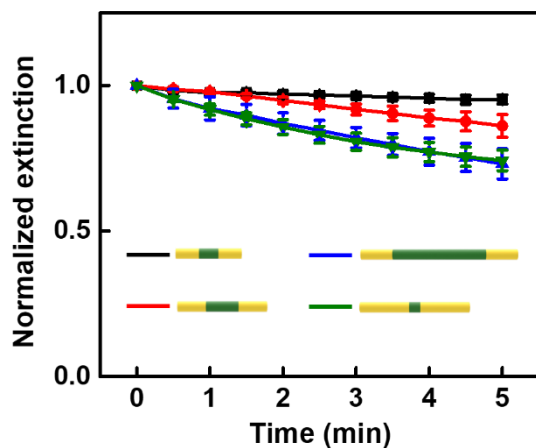


**Figure S5. Stability test of Au/Ni/Au nanorods with varying length of Au segment and Ni segment.** We monitored the extinction intensities of transverse mode of multiblock nanorods with different configurations through vis-NIR spectrophotometer. From the stability test, we confirmed that Au/Ni/Au NRs shown in Figure S3A showed best stability among the Au/Ni/Au NRs with varying geometrical parameters shown in Figure S3. When the lengths of Au segment or Ni segment of Au/Ni/Au NRs were larger than Au/Ni/Au nanorods in panel A, the extinction intensities of transverse mode of Au/Ni/Au NRs were consistently decreased as a function of time.

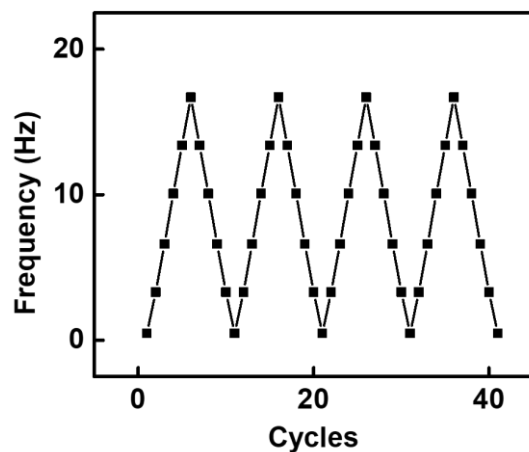


**Figure S6. Stability test of Au/Ni/Au NRs with varying lengths of Au segments and Ni segments shown in panel A in Fig. 2.** We consecutively increased and decreased the driving frequency of external rotating magnetic field from 15 rpm to 500 rpm for 17 min and measured the peak position of FTSPR spectra. Frequency peak position obtained from Au/Ni/Au NRs were reversibly varied from 0.5 Hz to 16.6 Hz, which rules out magnetic dipole induced aggregation among Au/Ni/Au NRs in solution.



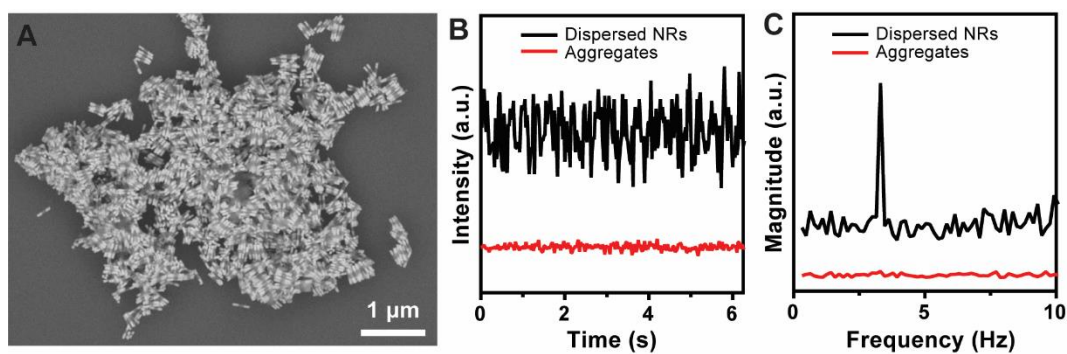


**Figure S7. Aggregated NRs do not provide FTSPR signals.** (A) We purposely induced aggregation of NRs by using 0.1 M dithiothreitol. Compared to dispersed NRs (i.e., not aggregated, black trace in (B-C)) showing the sine-function optical response as well as the clear FTSPR peak, the case of aggregates in red traces in (B-C) do not show any discernible signals.

## Supplementary Note 1. Measurement of viscosity of glycerol solution using commercial viscometers

We measured the viscosity of glycerol solution using Ubbelohde viscometer (VIS1030, Duksan general science) and Rotary viscometer (WVS-0.1M with spindle LV 1, Daihan scientific). We prepared the glycerol solutions with different viscosity by mixing glycerol (99.5 %, Sigma-Aldrich) and triply deionized water. The temperature was fixed at 25 °C using an air conditioning system during measurement since the viscosity of the glycerol solution is dependent on the temperature.

We measured the viscosity of 70%, 72%, and 74% glycerol solution using commercial rotary viscometer. The total volume of glycerol solution was fixed as 200 mL and measured for three times as shown below.

Volume fraction of glycerol	Measurement 1	Measurement 2	Measurement 3	Average
74 %	35.2 cP	35.4 cP	35.3 cP	35.3 ( $\pm 0.1$ ) cP
72 %	31.4 cP	31.2 cP	31.4 cP	31.3 ( $\pm 0.1$ ) cP
70 %	25.2 cP	25.4 cP	25.2 cP	25.3 ( $\pm 0.1$ ) cP

Then, to measure the viscosity of 0, 41, 55, 61, and 66% glycerol solution, we utilized Ubbelohde viscometer. The total volume of glycerol solution was fixed as 10 mL. We measured the time for 10 mL glycerol solution passing through the two marked lines of capillary of Ubbelohde viscometer, as shown in the table below. We conducted the measurement for three times.

Volume fraction of glycerol	Measurement 1	Measurement 2	Measurement 3
66 %	8954 s	8966 s	8958 s
61 %	6630 s	6639 s	6635 s
55 %	4527 s	4525 s	4510 s
41 %	2300 s	2325 s	2281 s
0 %	504 s	509 s	506 s

We calculated the viscosity of glycerol solution by following the previously reported literature.<sup>7</sup> Viscometer constant is calculated as follows:

$$\text{Viscometer constant} = \frac{\text{Absolute viscosity (cP)} \times \text{Efflux time (s)}}{\text{Density of solution (g/mL)}} = \frac{0.924 \times 0.997}{515} = 0.002$$

Using viscometer constant, we can calculate the viscosity of water-glycerol mixture as follows:

$$\text{Absolute viscosity (cP)} = \text{Viscometer constant} \times \text{Efflux time (s)} \times \text{Density of solution (g/mL)}$$

Volume fraction of glycerol	Density of glycerol solution (g/mL)	Measurement 1	Measurement 2	Measurement 3	Average
66 %	1.17	21.00 cP	21.03 cP	21.01 cP	21.01 ( $\pm 0.01$ ) cP
61 %	1.16	15.36 cP	15.38 cP	15.37 cP	15.37 ( $\pm 0.01$ ) cP
55 %	1.14	10.33 cP	10.33 cP	10.29 cP	10.32 ( $\pm 0.02$ ) cP
41 %	1.09	5.00 cP	5.06 cP	4.96 cP	5.01 ( $\pm 0.05$ ) cP
0 %	1.00	1.01 cP	1.02 cP	1.02 cP	1.02 ( $\pm 0.01$ ) cP

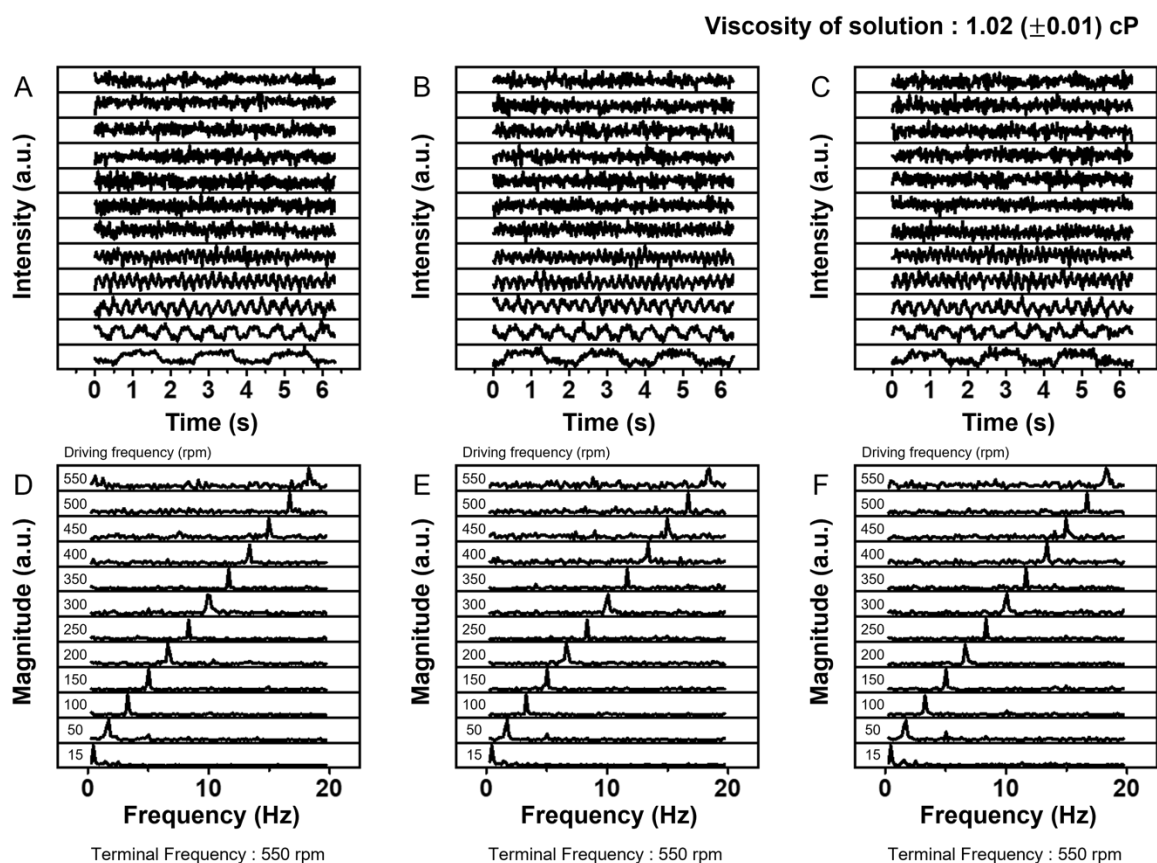


**Figure S8. Raw FTSPR data for viscosity measurement of water (viscosity =  $1.02 (\pm 0.01)$  cP).**

(A-C) Raw optical response data and (D-F) their corresponding frequency peak data after FFT.

Optical response data were obtained under driving frequencies from 15 rpm to 550 rpm at a measuring wavelength of 570 nm.

Viscosity of solution :  $5.01 (\pm 0.05)$  cP

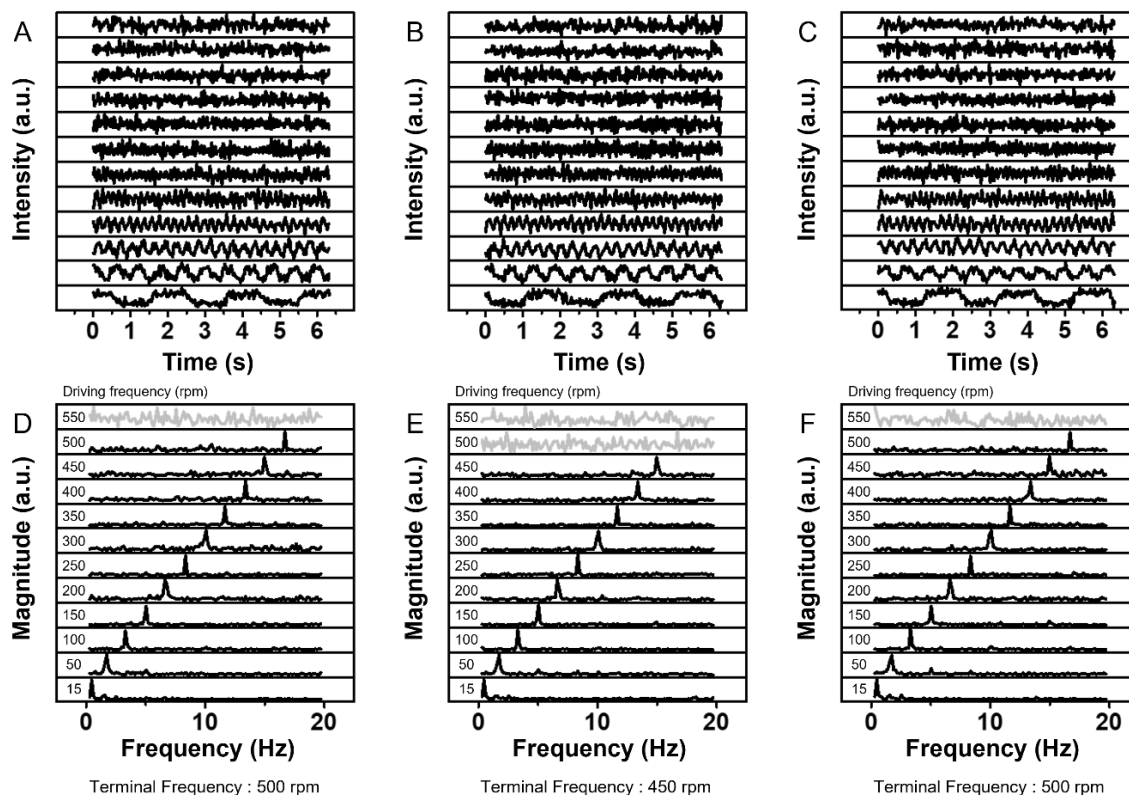


**Figure S9.** Raw FTSPR data for viscosity measurement of 41% glycerol solution (viscosity =  $5.01 (\pm 0.05)$  cP). (A-C) Raw optical response data and (D-F) their corresponding frequency peak data after FFT. Optical response data were obtained under driving frequencies from 15 rpm to 550 rpm at a measurement wavelength of 570 nm.

Viscosity of solution :  $10.32 (\pm 0.02)$  cP

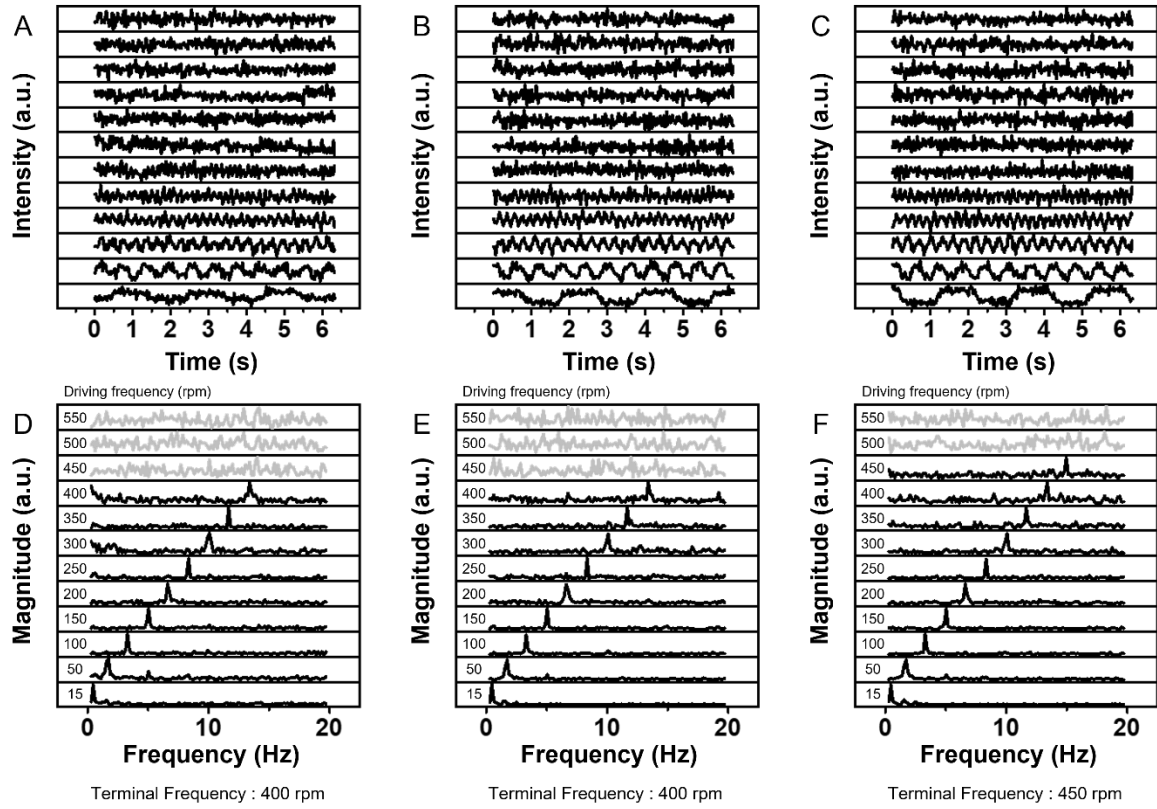


**Figure S10.** Raw FTSPR data for viscosity measurement of 55% glycerol solution (viscosity =  $10.32 (\pm 0.02)$  cP). (A-C) Raw optical response data and (D-F) their corresponding frequency peak data after FFT. Optical response data were obtained under driving frequencies from 15 rpm to 550 rpm at a measurement wavelength of 570 nm.

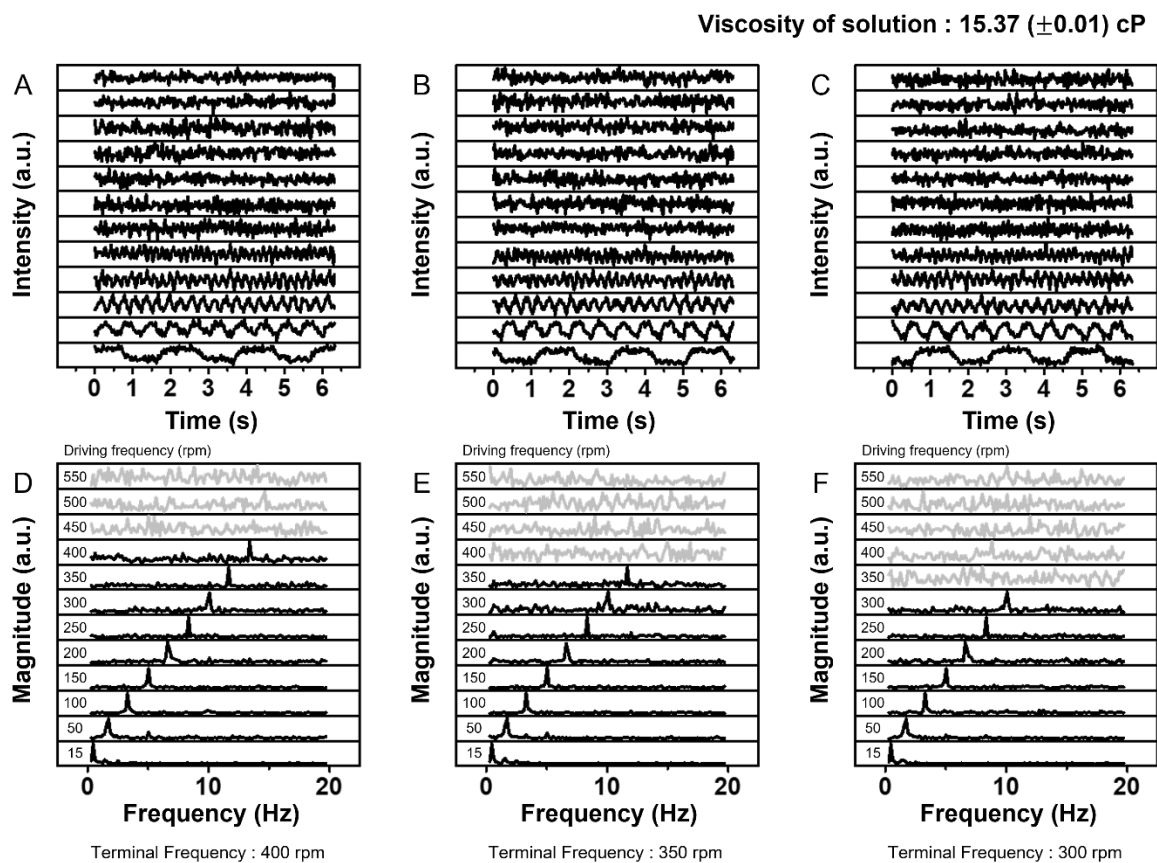


**Figure S11. Raw FTSPR data for viscosity measurement of 61% glycerol solution (viscosity = 15.37 ( $\pm 0.01$ ) cP). (A-C) Raw optical response data and (D-F) their corresponding frequency peak data after FFT. Optical response data were obtained under driving frequencies from 15 rpm to 550 rpm at a measurement wavelength of 570 nm.**

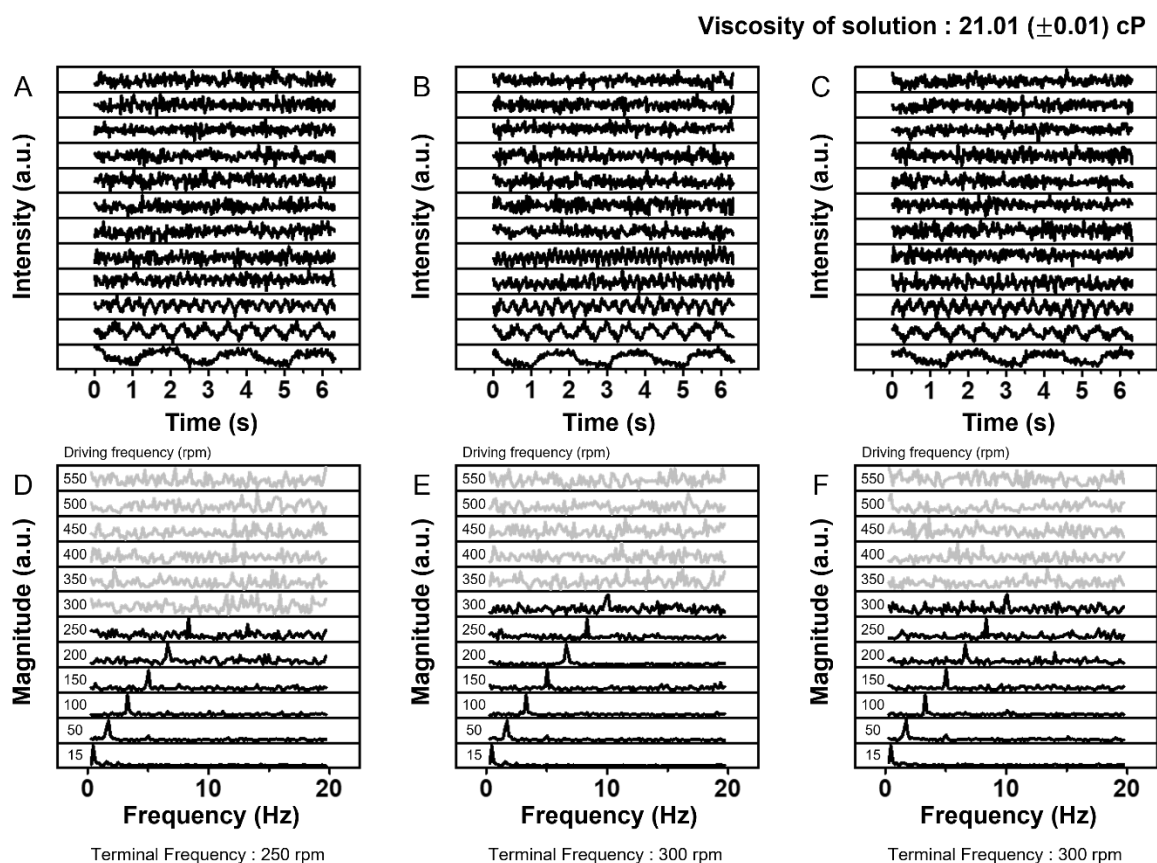


**Figure S12. Raw FTSPR data for viscosity measurement of 66% glycerol solution (viscosity = 21.01 ( $\pm 0.01$ ) cP). (A-C) Raw optical response data and (D-F) their corresponding frequency peak data after FFT. Optical response data were obtained under driving frequencies from 15 rpm to 550 rpm at a measurement wavelength of 570 nm.**



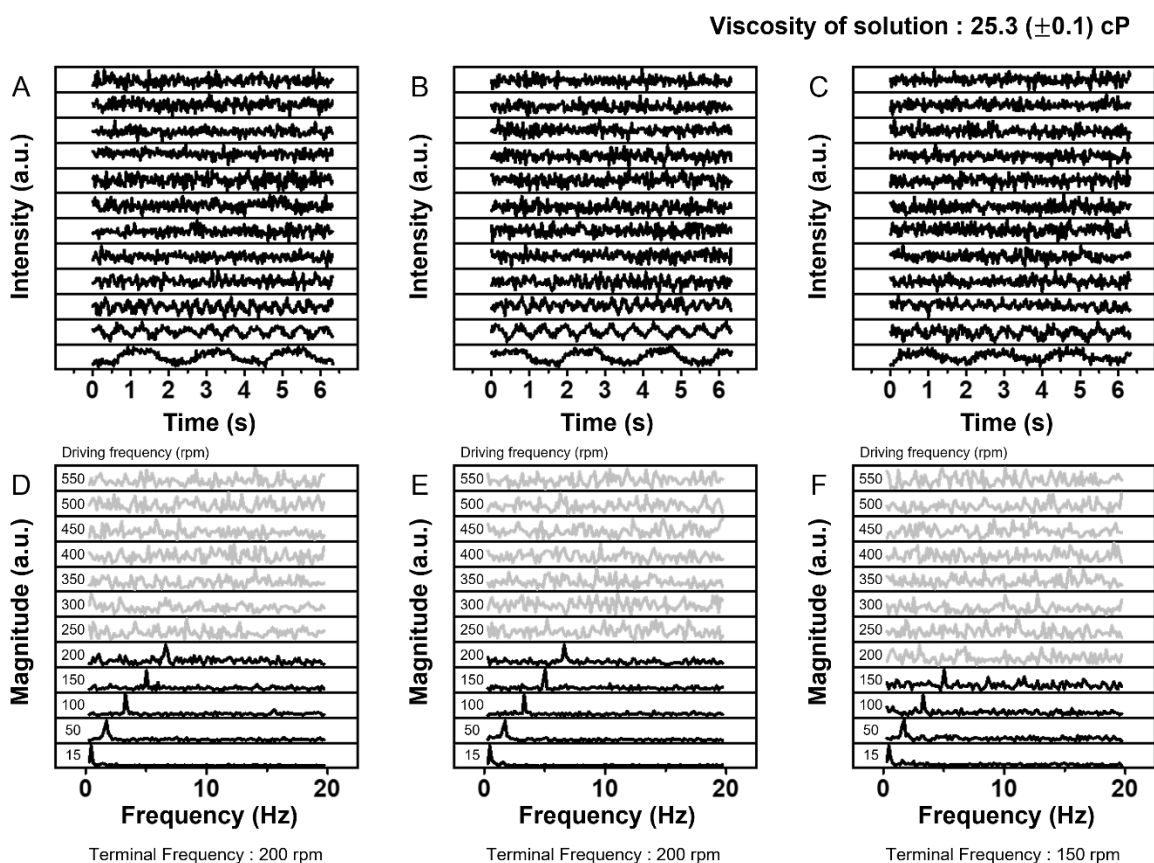


**Figure S13.** Raw FTSPR data for viscosity measurement of 70% glycerol solution (viscosity =  $25.3 (\pm 0.1)$  cP). (A-C) Raw optical response data and (D-F) their corresponding frequency peak data after FFT. Optical response data were obtained under driving frequencies from 15 rpm to 550 rpm at a measurement wavelength of 570 nm.

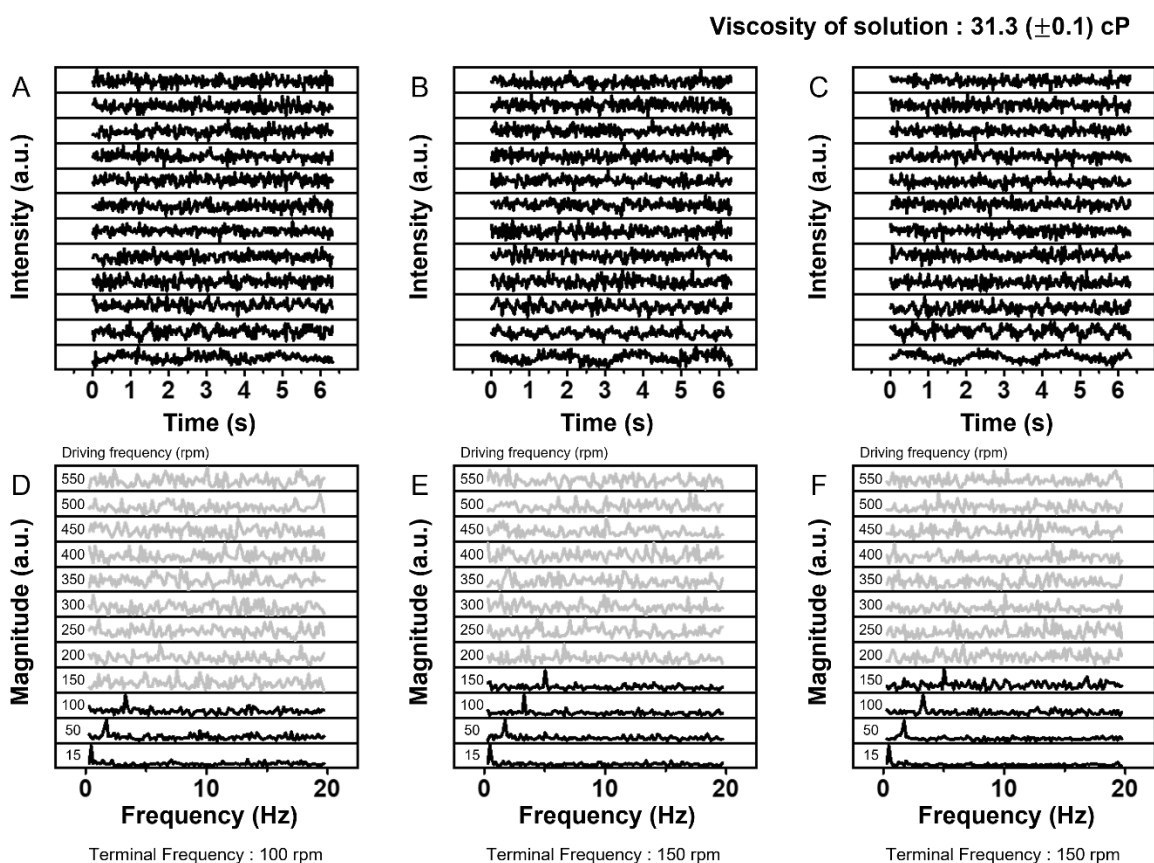


**Figure S14.** Raw FTSPR data for viscosity measurement of 72% glycerol solution (viscosity =  $31.3 (\pm 0.1)$  cP). (A-C) Raw optical response data and (D-F) their corresponding frequency peak data after FFT. Optical response data were obtained under driving frequencies from 15 rpm to 550 rpm at a measurement wavelength of 570 nm.

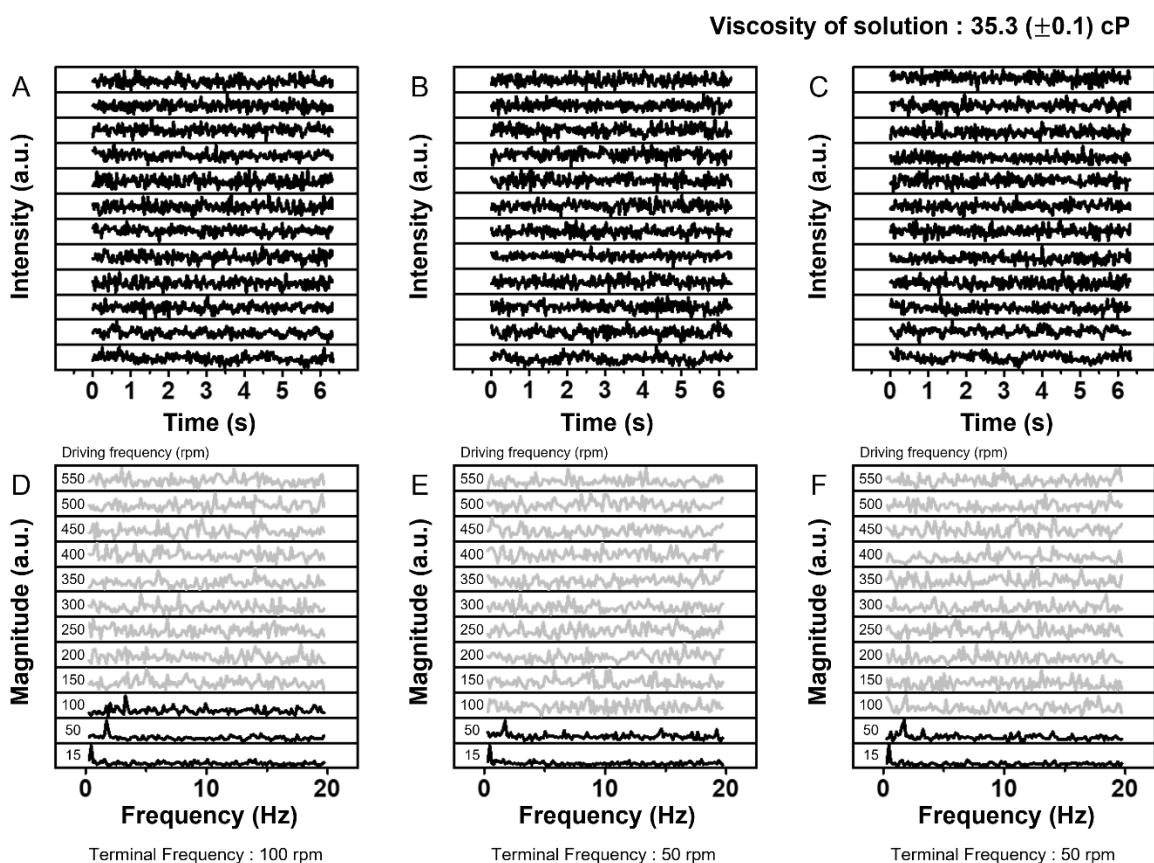


**Figure S15.** Raw FTSPR data for viscosity measurement of 74% glycerol solution (viscosity =  $35.3 (\pm 0.1)$  cP). (A-C) Raw optical response data and (D-F) their corresponding frequency peak data after FFT. Optical response data were obtained under driving frequencies from 15 rpm to 550 rpm at a measurement wavelength of 570 nm.

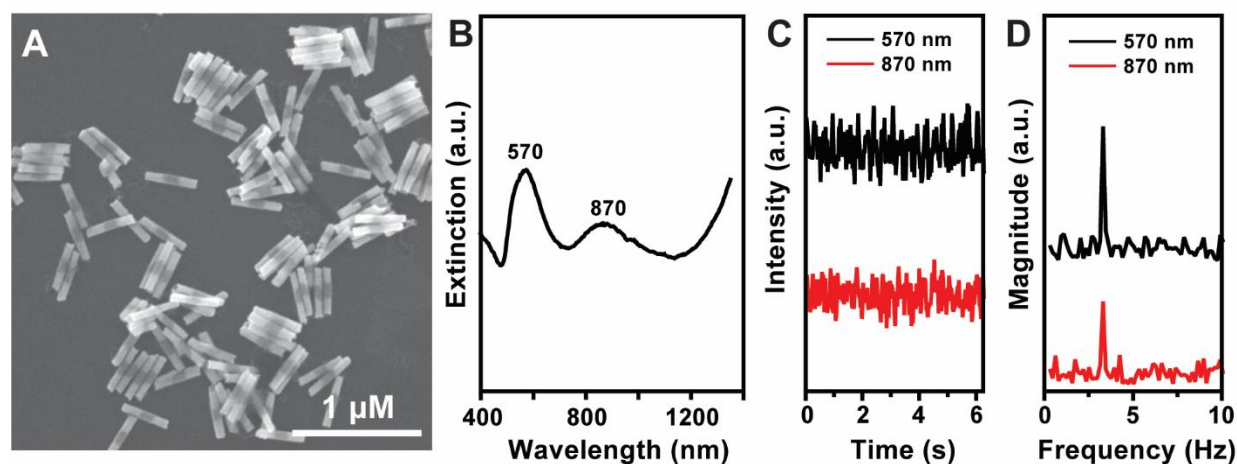


**Figure S16. Optimization of monitoring wavelength for Fourier transform surface plasmon resonance (FTSPR) of Au/Ni/Au nanorods.** (A) A FE-SEM image, and (B) corresponding visible and near-infrared (vis-NIR) spectrum of Au/Ni/Au nanorods. Au/Ni/Au nanorods shown in panel A represent transverse mode and quadrupole longitudinal mode at 570 nm and 870 nm, respectively. (C) We performed magnetic modulation of Au/Ni/Au nanorods at a monitoring wavelength of 570 nm (black trace) and 870 nm (red trace). (D) The intensity of the FTSPR peak measured at 570 nm was higher than that measured at 870 nm providing higher sensitivity for the FTSPR measurement.

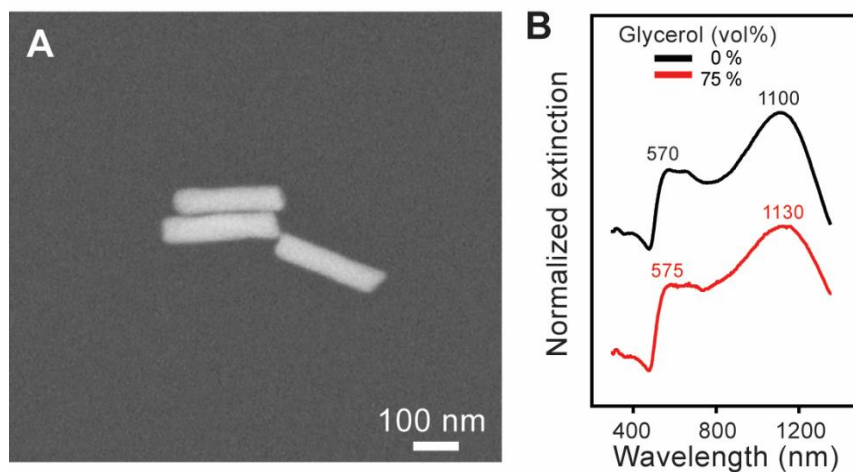
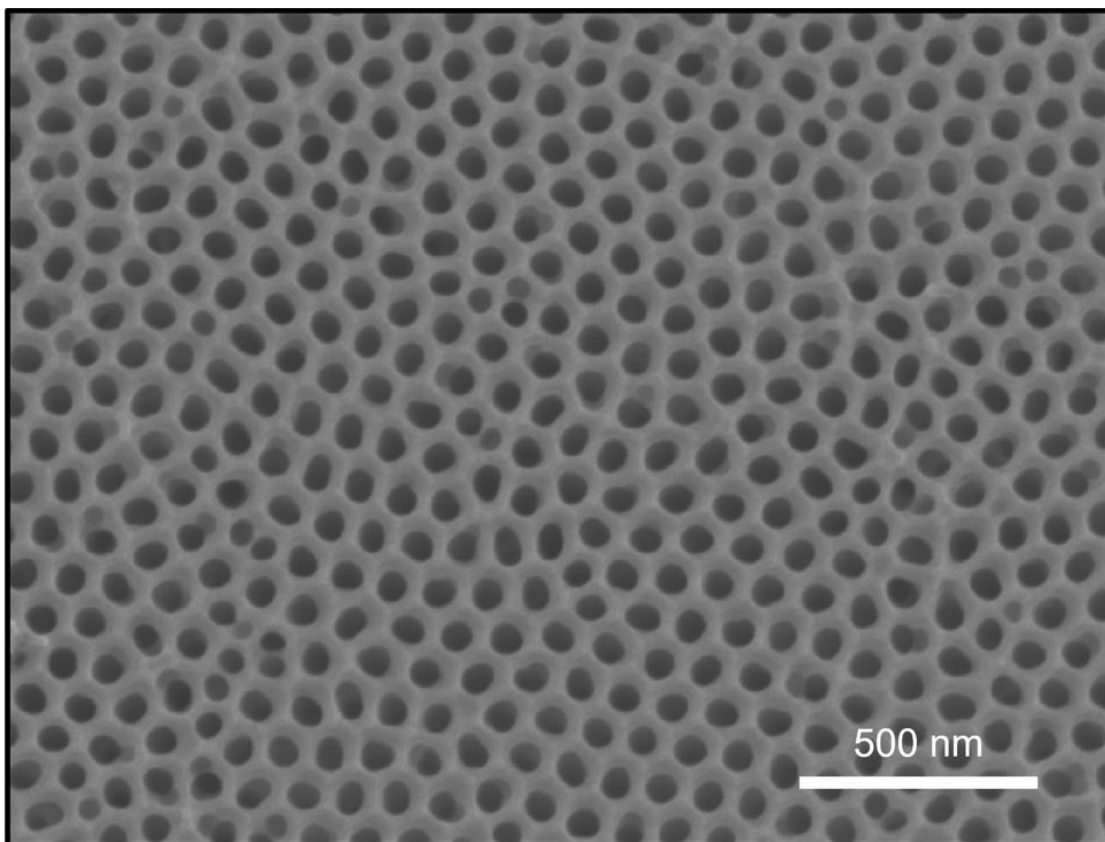


**Figure S17. A FE-SEM image of single-component Au nanorods, and their corresponding vis-NIR spectra dispersed in 0% (water) and 75% glycerol solution. (A)** A FE-SEM image of Au nanorods. **(B)** We monitored the vis-NIR spectra of Au nanorods shown in panel A dispersed in 0% (water, black trace) and 75% glycerol solution (mixed with water, red trace). With the increased volume fraction of glycerol in a glycerol-water mixture, both the transverse mode and longitudinal mode of Au nanorods were red-shifted. The longitudinal mode was more sensitive to the surrounding refractive index change than transverse mode. Given that the extinction intensity at the monitoring wavelength affects FTSPR peak intensity as shown in **Figure S14**, we chose transverse mode, which is insensitive to the change in surrounding refractive index as a monitoring wavelength for glycerol solution and intracellular viscosity measurements.

## Supplementary Note 2. The estimation of the concentration of Au/Ni/Au nanorods



We estimated the concentration of Au/Ni/Au nanorods as follows. We obtained the FE-SEM image of anodized aluminum oxide (AAO) template (*vide supra*) and counted the number of pores shown in the FE-SEM image, which was 457.

The area of FE-SEM image:

$$\text{The area of a SEM image} = 2.31 \mu\text{m} \times 1.74 \mu\text{m} = 4.02 \mu\text{m}^2$$

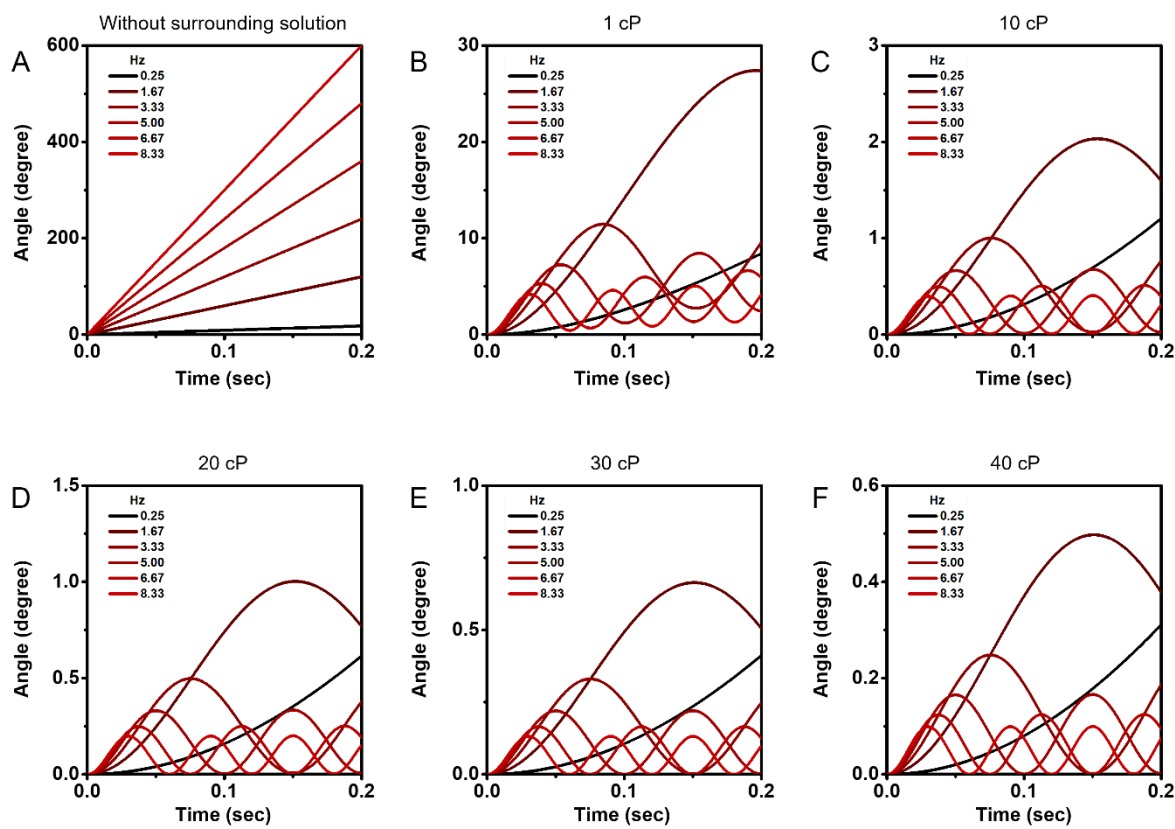
The total area of AAO:

$$\text{The total area of AAO} = 4500 \mu\text{m} \times 4500 \mu\text{m} \times \pi = 63617251 \mu\text{m}^2$$

Therefore, the number of nanorods from one AAO template is as follows:

The number of nanorods from one AAO template =



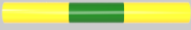


$$\frac{\text{The number of pores} \times \text{The total area of AAO}}{\text{The area of a SEM image}} = \frac{457 \times 63617251}{4.02} = 10 \text{ fmol}$$



**Figure S18. FEM simulation for the dynamics of Au/Ni/Au NRs (dimension: diameter = 74 nm, 174-145-174 nm) under the condition of without and with surrounding medium with different viscosities (1, 10, 20, 30 and 40 cP) and driving frequencies (from 0.25 to 8.33 Hz).** The angular displacement of Au/Ni/Au NRs (dimension: diameter = 74 nm, 174-145-174 nm) as a function of time under the varying driving frequency **(A)** without any external perturbation surrounding Au/Ni/Au NRs and with surrounding medium of **(B)** 1 cP, **(C)** 10 cP, **(D)** 20 cP, **(E)** 30 cP, and **(F)** 40 cP viscosities.

### Supplementary Note 3. Critical frequency of Au/Ni/Au nanorods with different configuration of component

When we increased the length of Ni segments from 145 to 301 and 393 nm while fixing the total length to be the same (493 nm), NRs rotate well even in a higher viscosity solution, indicating that a NR with a Ni length longer than 145 nm results in a lower sensitivity of terminal frequency-based sensing (**Figure S18-S22**). On the other hand, NRs with 71-nm and 31-nm Ni segments showed almost negligible angular displacement under the viscous solution. These results imply that the rotational dynamics of NRs along with hydrodynamic forces can be magnetically modulated and multiblock NRs can be rationally designed for the viscosity of target fluids.

	Length (Au segment)	Length (Ni segment)	Total length	Diameter
Sample A 	50 nm	393 nm	493 nm	74 nm
Sample B 	96 nm	301 nm	493 nm	74 nm
Sample C 	174 nm	145 nm	493 nm	74 nm
Sample D 	211 nm	71 nm	493 nm	74 nm
Sample E 	231 nm	31 nm	493 nm	74 nm

**Figure S19. Physical dimensions of Au-Ni-Au nanorods for theoretical simulation.** The length of Au segments, the length of Ni segments, total length, and diameter of Au-Ni-Au nanorods for theoretical simulation are shown above.



Au-Ni-Au dimension: 50-393-50 (nm)

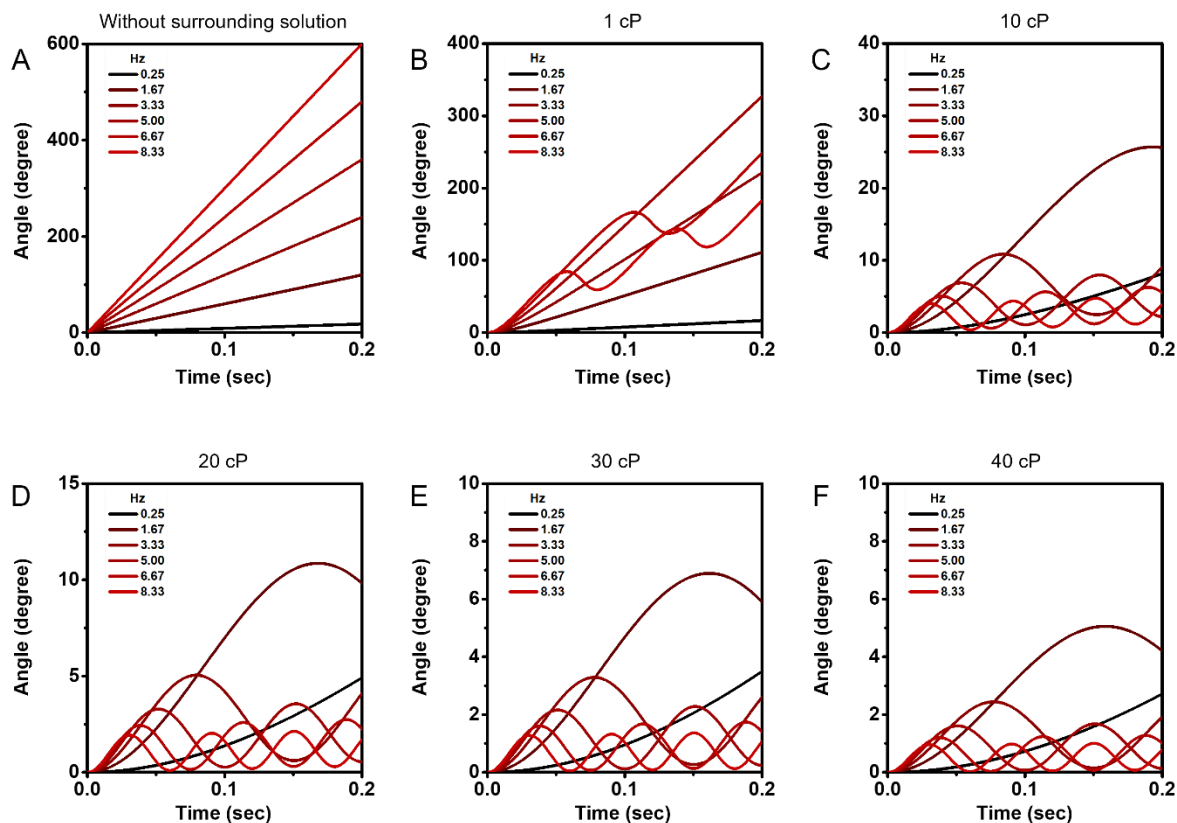


**Figure S20.** FEM simulation for the dynamics of Au/Ni/Au NRs (dimension: diameter = 74 nm, 50-393-50 nm) under the condition of without and with surrounding medium of different viscosities (1, 10, 20, 30 and 40 cP) and driving frequencies (from 0.25 to 8.33 Hz). The angular displacement of Au/Ni/Au NRs (dimension: diameter = 74 nm, 50-393-50 nm) as a function of time under the varying driving frequency (A) without any external perturbation surrounding Au/Ni/Au NRs and with surrounding medium of (B) 1 cP, (C) 10 cP, (D) 20 cP, (E) 30 cP, and (F) 40 cP viscosities.

Au-Ni-Au dimension: 96-301-96 (nm)

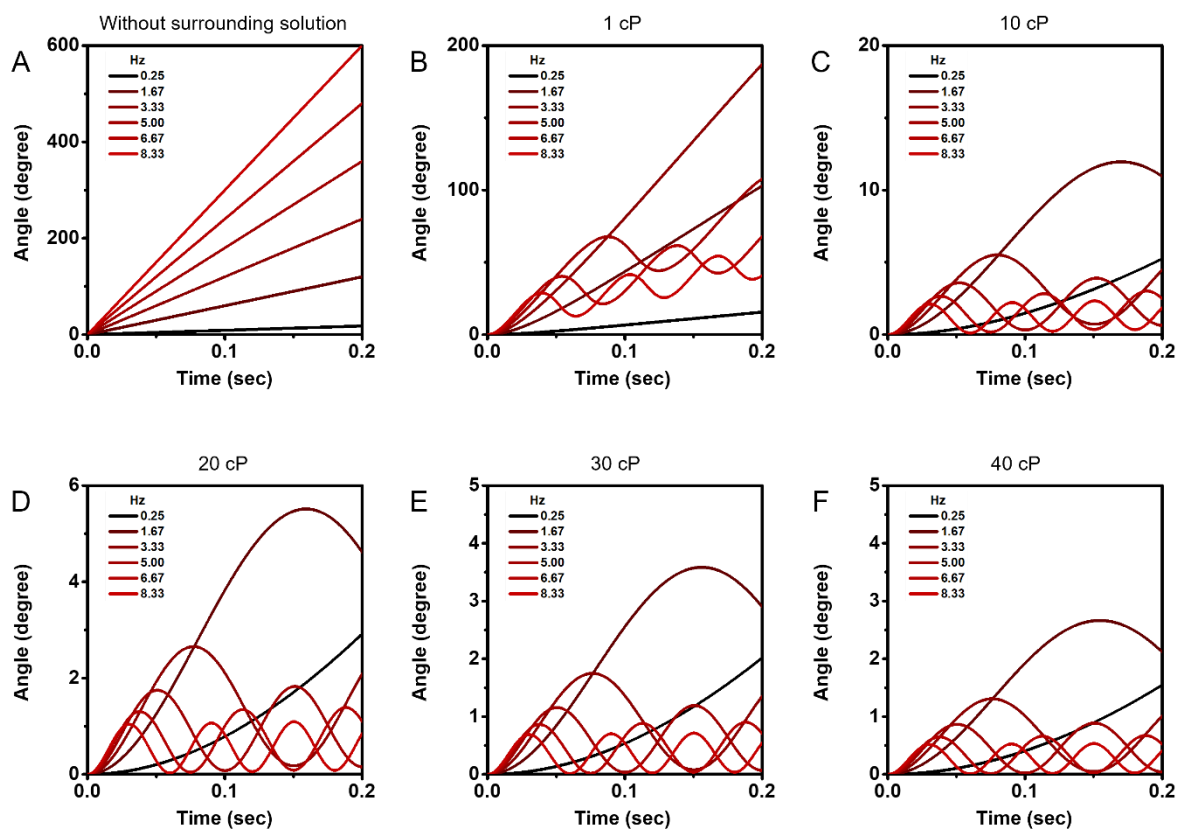


**Figure S21. FEM simulation for the dynamics of Au/Ni/Au NRs (dimension: diameter = 74 nm, 96-301-96 nm) under the condition of without and with surrounding medium of different viscosities (1, 10, 20, 30 and 40 cP) and driving frequencies (from 0.25 to 8.33 Hz). The angular displacement of Au/Ni/Au NRs (dimension: diameter 74 nm, 96-301-96 nm) as a function of time under the varying driving frequency (A) without any external perturbation surrounding Au/Ni/Au NRs and with surrounding medium of (B) 1 cP, (C) 10 cP, (D) 20 cP, (E) 30 cP, and (F) 40 cP viscosities**

Au-Ni-Au dimension: 211-71-211 (nm)

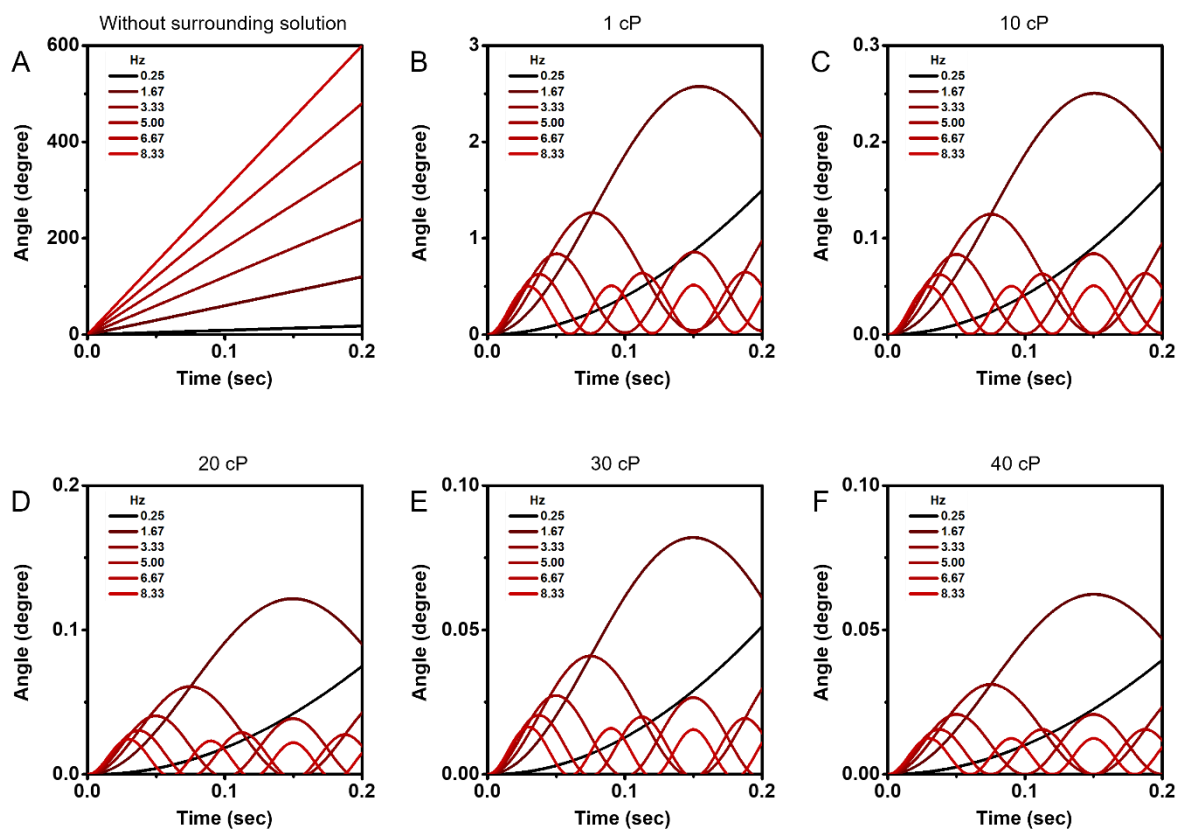


**Figure S22. FEM simulation for the dynamics of Au/Ni/Au NRs (dimension: diameter = 74 nm, 211-71-211 nm) under the condition of without and with surrounding medium of different viscosities (1, 10, 20, 30 and 40 cP) and driving frequencies (from 0.25 to 8.33 Hz).** The angular displacement of Au/Ni/Au NRs (dimension: diameter = 74 nm, 211-71-211 nm) as a function of time under the varying driving frequency (A) without any external perturbation surrounding Au/Ni/Au NRs and with surrounding medium of (B) 1 cP, (C) 10 cP, (D) 20 cP, (E) 30 cP, and (F) 40 cP viscosities.

Au-Ni-Au dimension: 231-31-231 (nm)

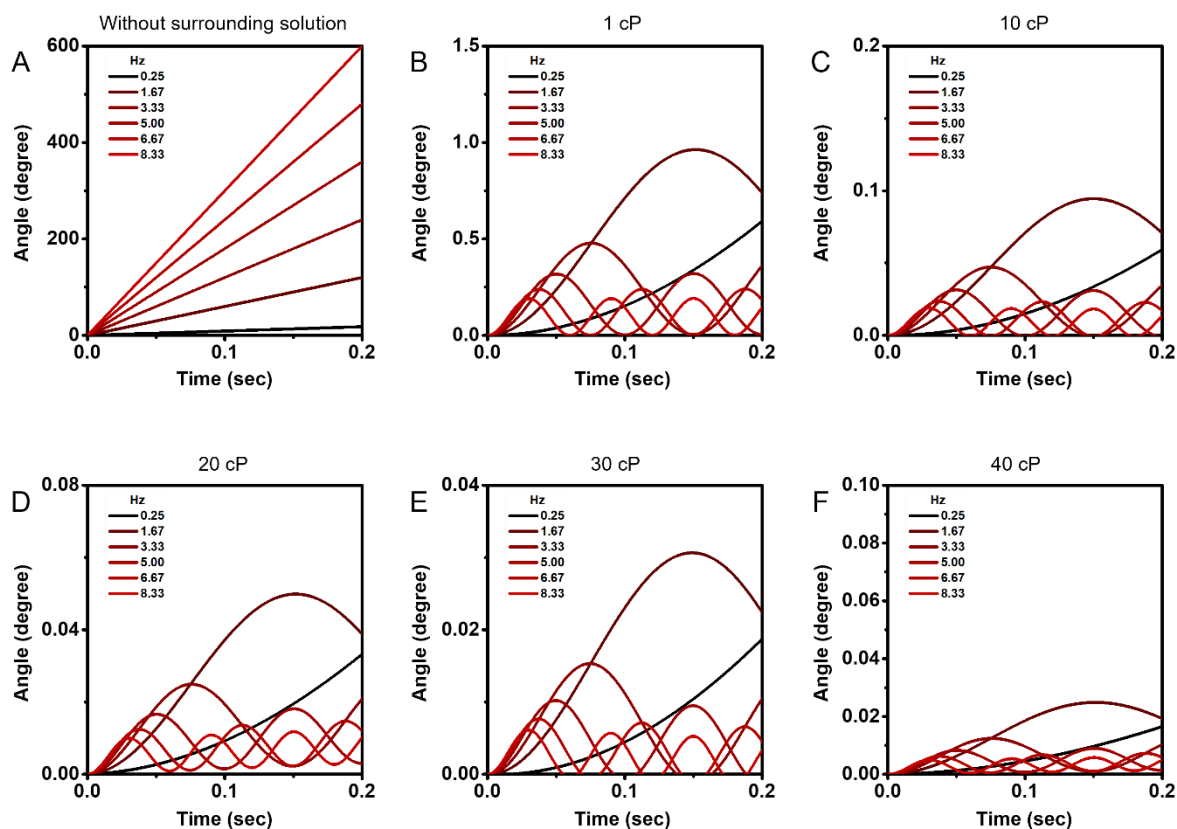


**Figure S23. FEM simulation for the dynamics of Au/Ni/Au NRs (dimension: diameter = 74 nm, 231-31-231 nm) under the condition of without and with surrounding medium with different viscosities (1, 10, 20, 30 and 40 cP) and driving frequencies (from 0.25 to 8.33 Hz).** The angular displacement of Au/Ni/Au NRs (dimension: diameter = 74 nm, 231-31-231 nm) as a function of time under the varying driving frequency (A) without any external perturbation surrounding Au/Ni/Au NRs and with viscous surrounding medium with (B) 1 cP, (C) 10 cP, (D) 20 cP, (E) 30 cP, and (F) 40 cP viscosities.

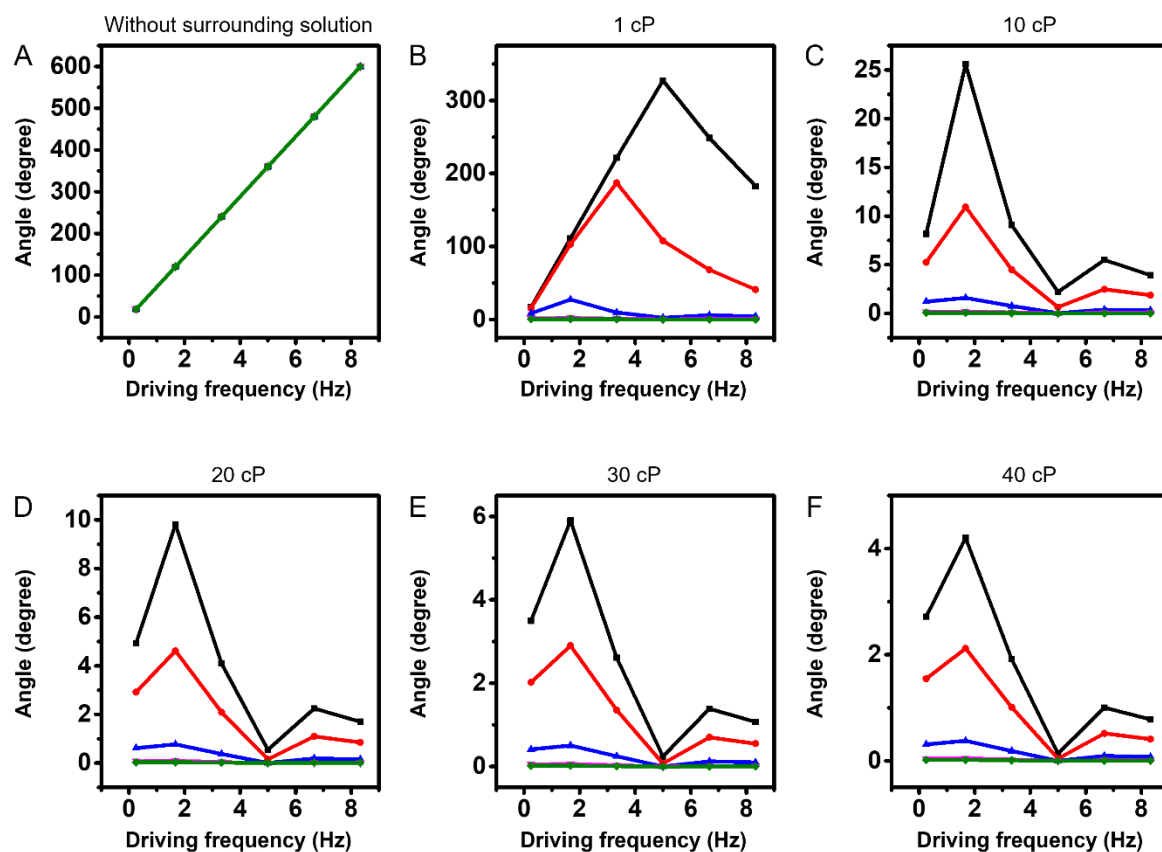


**Figure S24. Angular displacement of Au/Ni/Au NRs with different physical dimensions at a fixed time point (0.2 sec) as a function of driving frequency for different solution viscosities.** The angular displacement of Au/Ni/Au NRs with different physical dimensions at a fixed time point (0.2 sec) under the varying driving frequency **(A)** without any external perturbation surrounding Au/Ni/Au NRs and with surrounding medium with **(B)** 1 cP, **(C)** 10 cP, **(D)** 20 cP, **(E)** 30 cP, and **(F)** 40 cP viscosities.

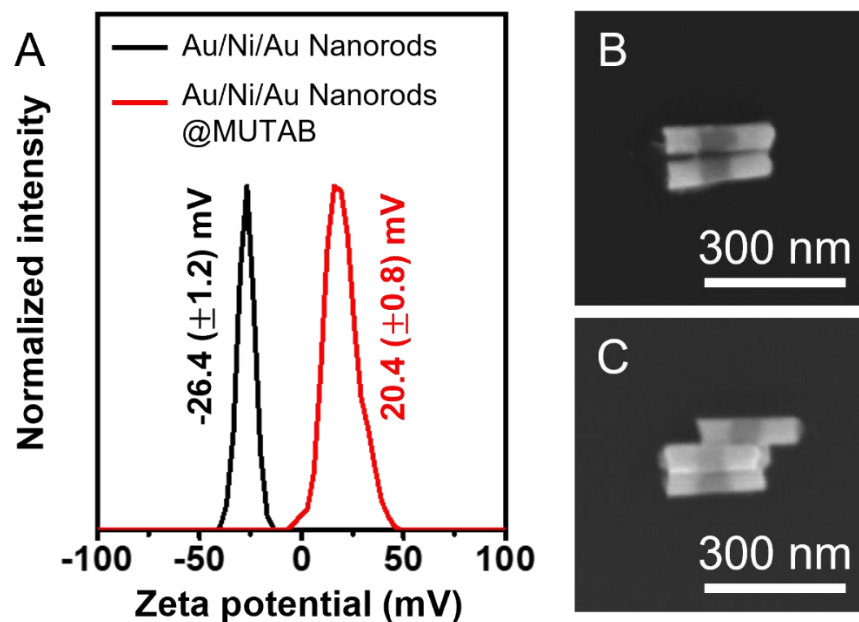


**Figure S25. Zeta potential data and FE-SEM images of Au/Ni/Au nanorods before and after surface modification with MUTAB.** (A) Zeta potential data of Au/Ni/Au nanorods before (black trace) and after (red trace) surface modification with MUTAB. Bare Au/Ni/Au nanorods exhibited a negative zeta potential of  $-26.4 (\pm 1.2)$  mV due to the hydroxides coated at the surface of Ni segments. After surface modification with MUTAB, the zeta potential was shifted to  $+20.4 (\pm 0.8)$  mV, which is attributed to the presence of positively charged tetramethylammonium functional groups of MUTAB. We obtained FE-SEM images of Au/Ni/Au nanorods (B) before and (C) after MUTAB treatments that did not induce any structural deformation in the Au/Ni/Au nanorods.

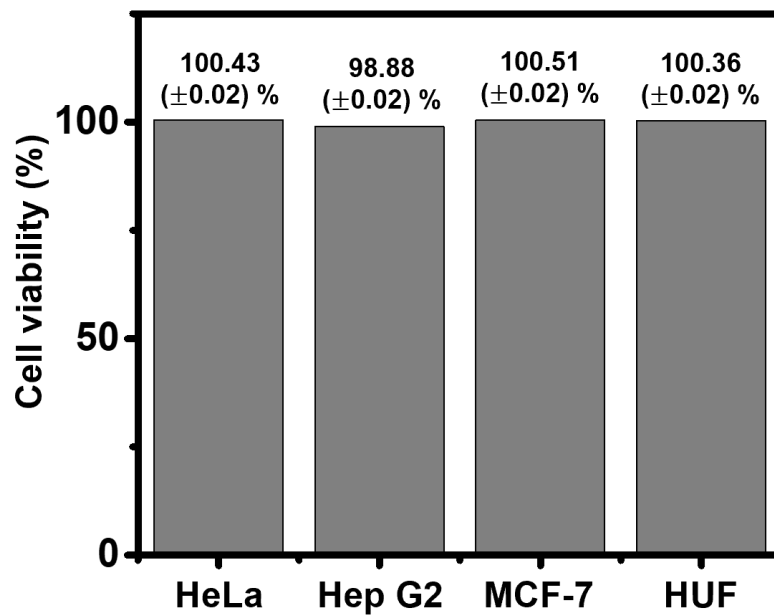


**Figure S26. MTT assay results for cell cytotoxicity of Au/Ni/Au nanorods in HeLa, Hep G2, MCF-7, and HUF cells.** From the MTT assay, the cell viability of Au/Ni/Au nanorods in HeLa, Hep G2, MCF-7, and HUF cells was higher than 98%, showing high biocompatibility.

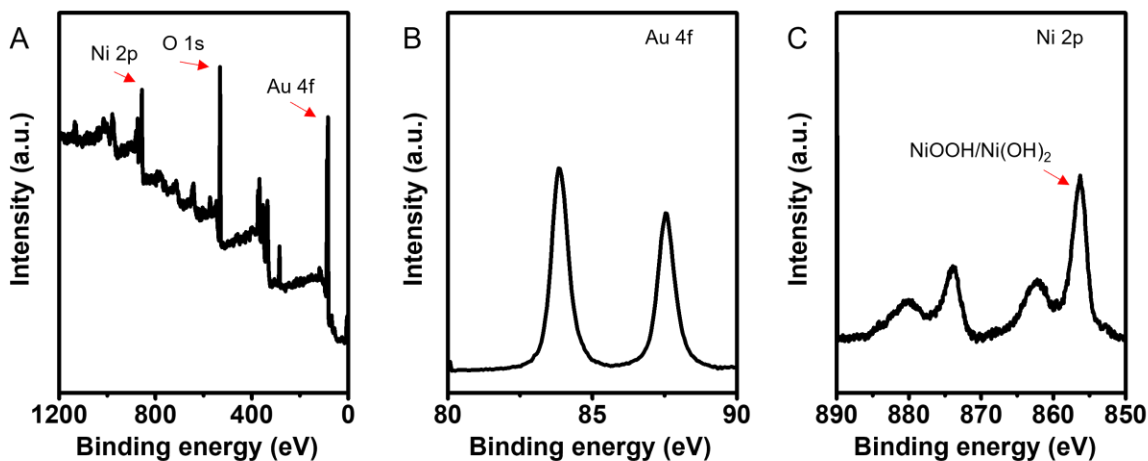


**Figure S27. X-ray photoelectron spectroscopy (XPS) analysis of Au/Ni/Au nanorods.** (A) XPS spectrum of Au/Ni/Au nanorods. For XPS measurement, a film of Au/Ni/Au nanorods was fabricated on the silicon wafer by dropping the suspension of Au/Ni/Au nanorods. (B) XPS spectra of Au 4f and (C) Ni 2p from Au/Ni/Au nanorods. In the Au 4f spectrum, no shoulder peaks were found due to the oxidation-resistant Au segments.<sup>8</sup> From Ni 2p spectrum, the peak at 856 eV was shown, indicating that NiOOH/Ni(OH)<sub>2</sub> formed at the surface of Ni segments of Au/Ni/Au nanorods.



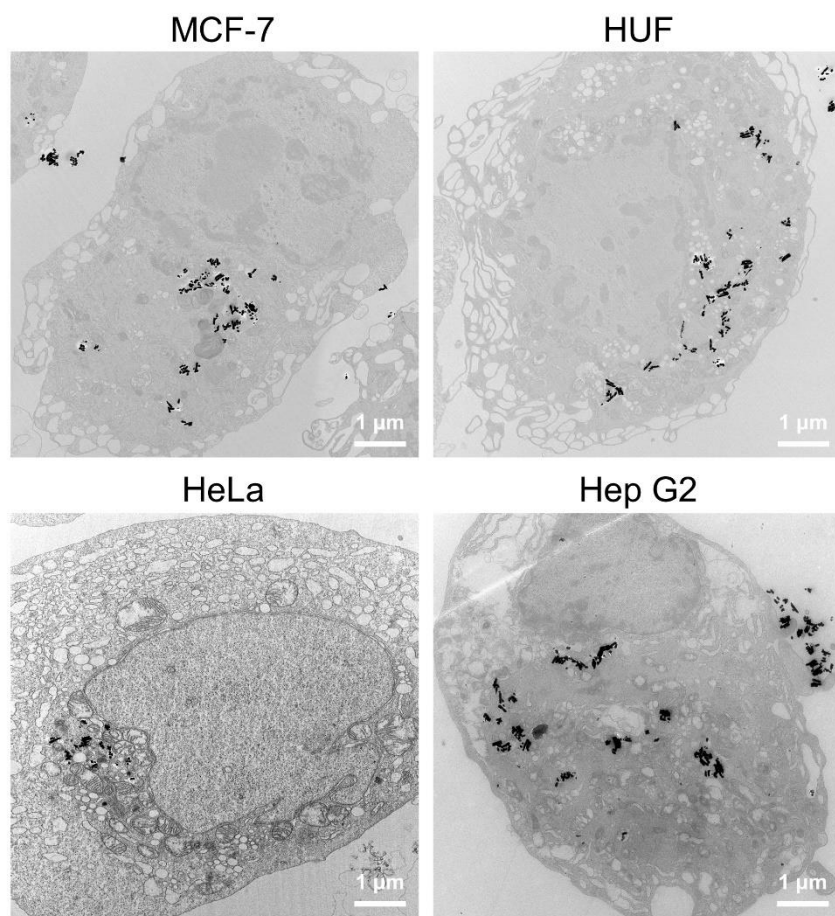


**Figure S28. Localization of Au/Ni/Au NRs in living cells.** TEM images of Au/Ni/Au NRs inside four different cell lines (MCF-7, HUF, HeLa and Hep G2).

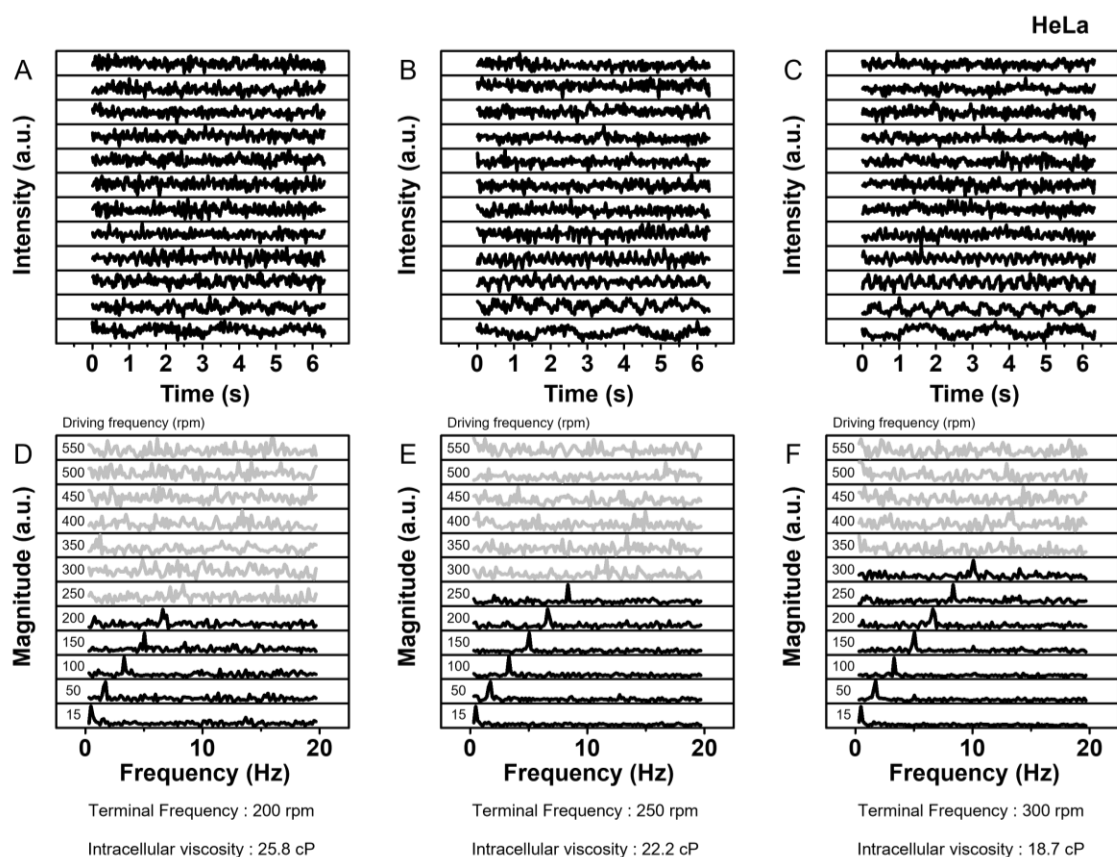


**Figure S29. Raw FTSPR data for viscosity measurement of HeLa cells (measurement 1, 2, and 3). (A-C) Raw optical response data and (D-F) their corresponding frequency peak data after FFT. Optical response data were obtained under driving frequencies from 15 rpm to 550 rpm at a measurement wavelength of 570 nm.**

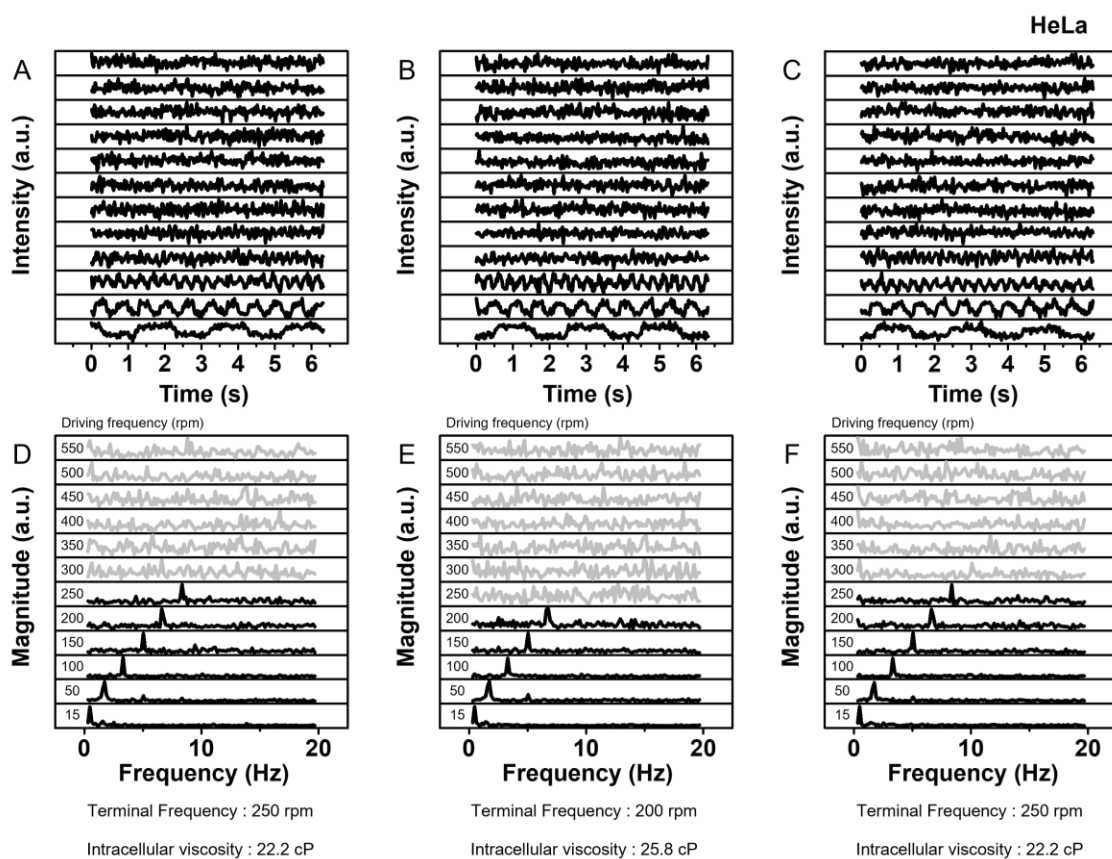


**Figure S30. Raw FTSPR data for viscosity measurement of HeLa cells (measurement 4, 5, and 6). (A-C) Raw optical response data and (D-F) their corresponding frequency peak data after FFT. Optical response data were obtained under driving frequencies from 15 rpm to 550 rpm at a measurement wavelength of 570 nm.**

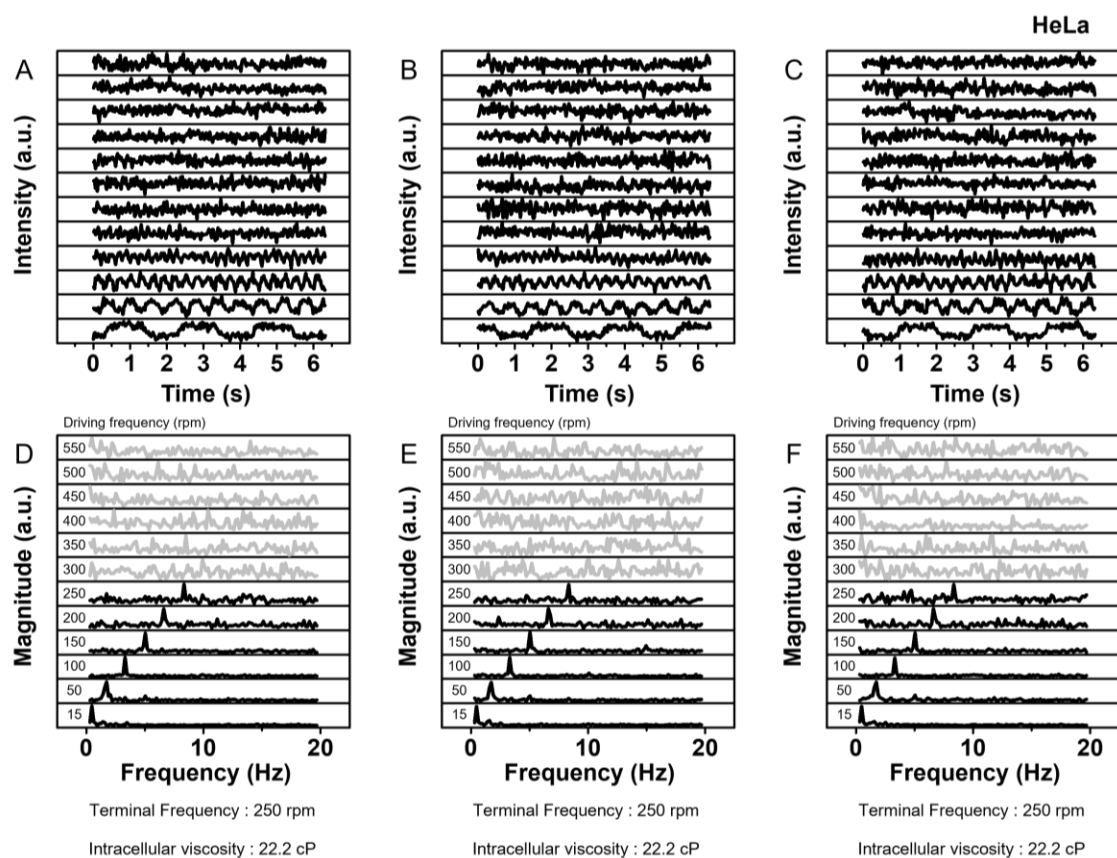
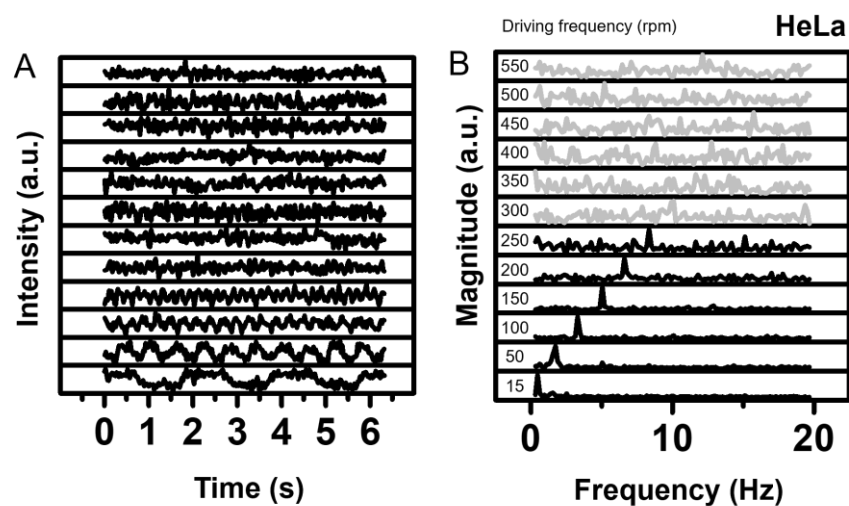


**Figure S31. Raw FTSPR data for viscosity measurement of HeLa cells (measurement 7, 8, and 9). (A-C) Raw optical response data and (D-F) their corresponding frequency peak data after FFT. Optical response data were obtained under driving frequencies from 15 rpm to 550 rpm at a measurement wavelength of 570 nm.**



Terminal Frequency : 250 rpm

Intracellular viscosity : 22.2 cP

**Figure S32. Raw FTSPR data for viscosity measurement of HeLa cells (measurement 10).** (A) Raw optical response data and (B) their corresponding frequency peak data after FFT. Optical response data were obtained under driving frequencies from 15 rpm to 550 rpm at a measurement wavelength of 570 nm.

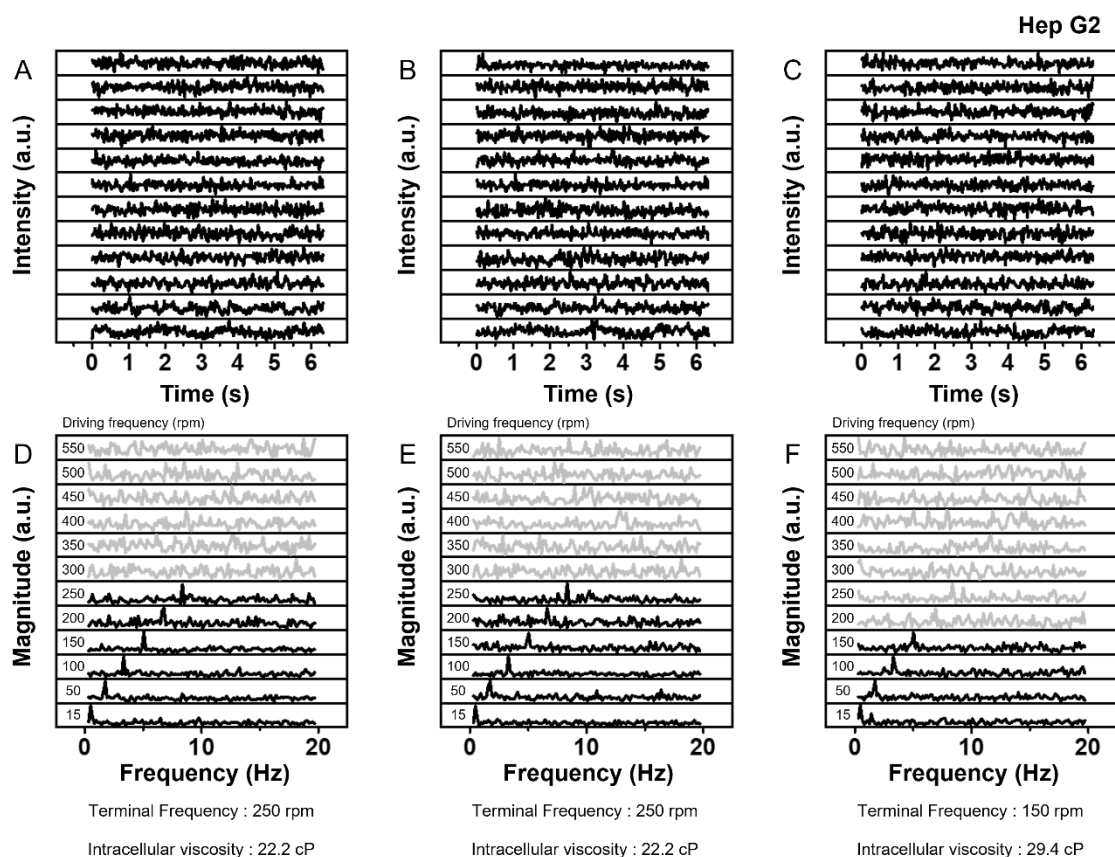


**Figure S33. Raw FTSPR data for viscosity measurement of Hep G2 cells (measurement 1, 2, and 3). (A-C) Raw optical response data and (D-F) their corresponding frequency peak data after FFT. Optical response data were obtained under driving frequencies from 15 rpm to 550 rpm at a measurement wavelength of 570 nm.**

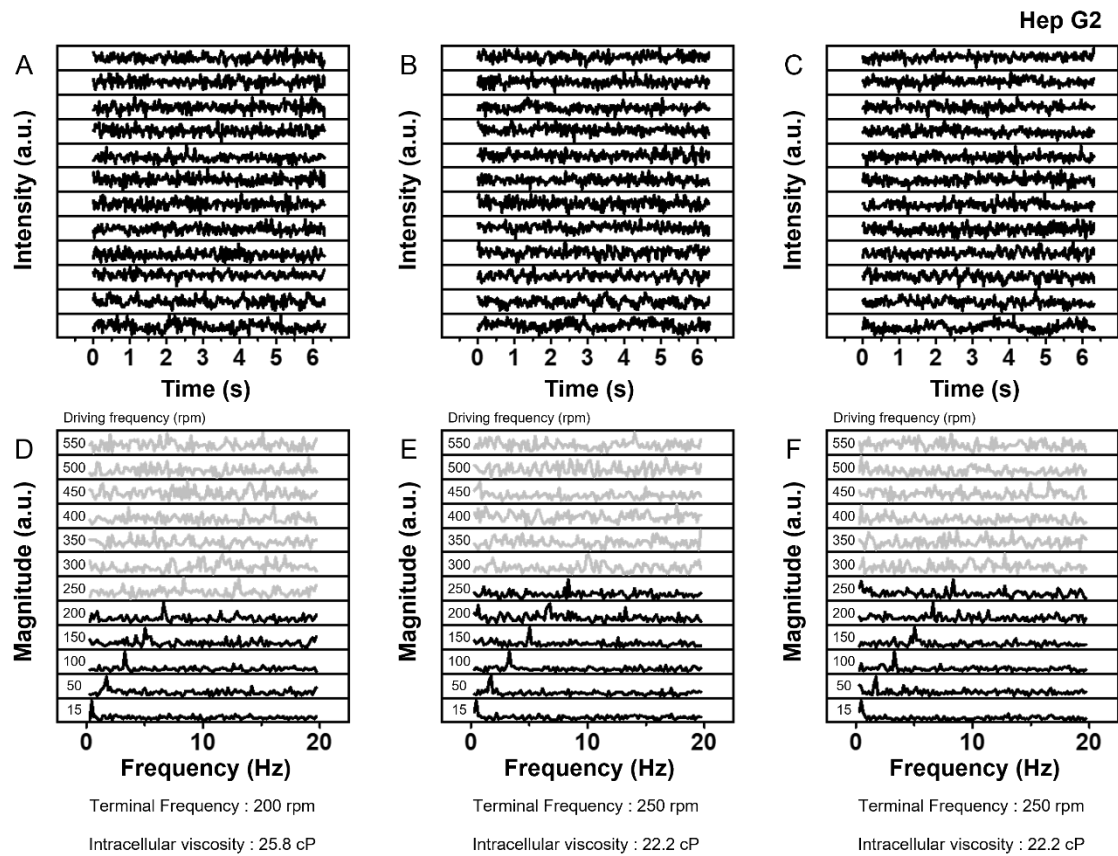


**Figure S34. Raw FTSPR data for viscosity measurement of Hep G2 cells (measurement 4, 5, and 6). (A-C) Raw optical response data and (D-F) their corresponding frequency peak data after FFT. Optical response data were obtained under driving frequencies from 15 rpm to 550 rpm at a measurement wavelength of 570 nm.**

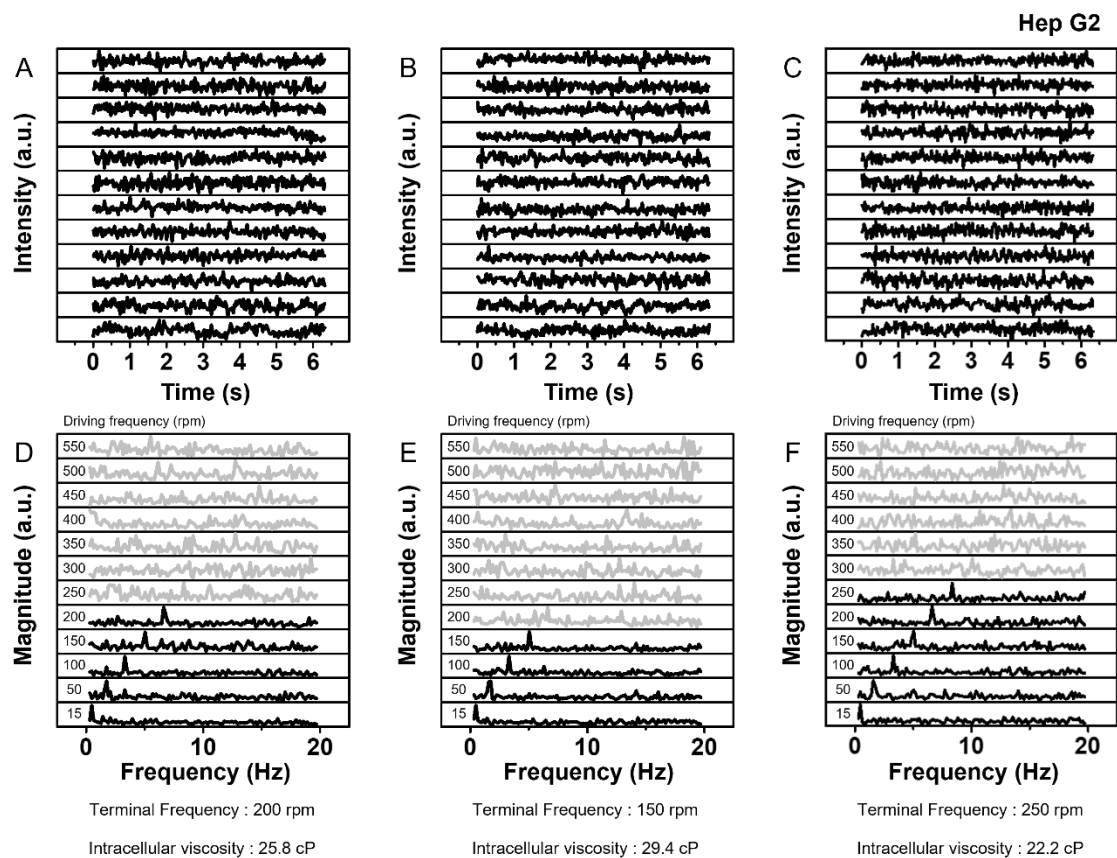
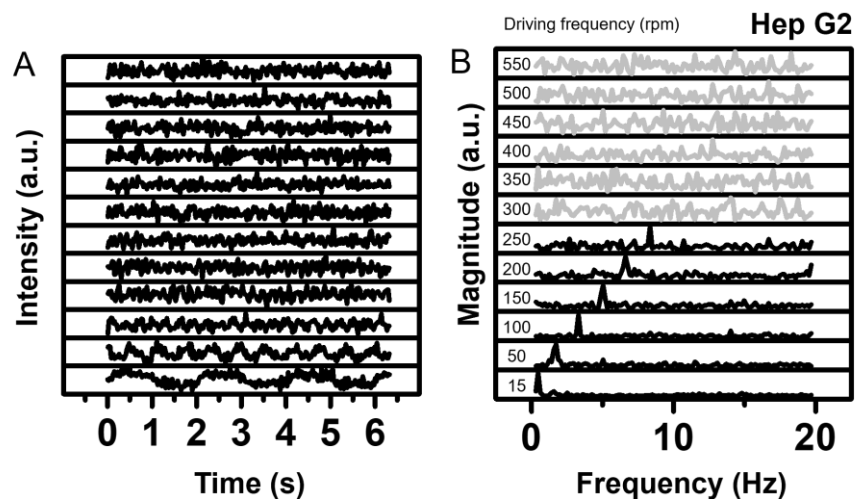


**Figure S35. Raw FTSPR data for viscosity measurement of Hep G2 cells (measurement 7, 8, and 9). (A-C) Raw optical response data and (D-F) their corresponding frequency peak data after FFT. Optical response data were obtained under driving frequencies from 15 rpm to 550 rpm at a measurement wavelength of 570 nm.**





Terminal Frequency : 250 rpm

Intracellular viscosity : 22.2 cP

**Figure S36. Raw FTSPR data for viscosity measurement of Hep G2 cells (measurement 10).**

**(A)** Raw optical response data and **(B)** their corresponding frequency peak data after FFT. Optical response data were obtained under driving frequencies from 15 rpm to 550 rpm at a measurement wavelength of 570 nm.

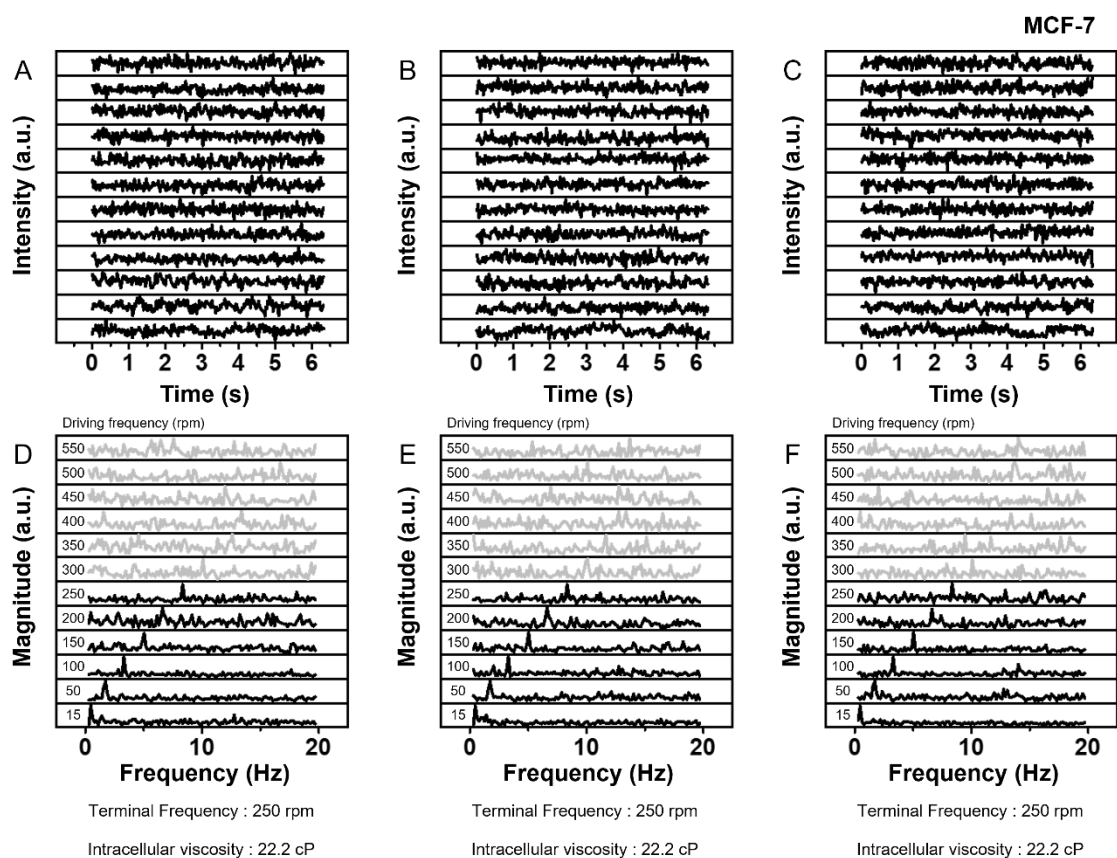


**Figure S37. Raw FTSPR data for viscosity measurement of MCF-7 cells (measurement 1, 2, and 3). (A-C) Raw optical response data and (D-F) their corresponding frequency peak data after FFT. Optical response data were obtained under driving frequencies from 15 rpm to 550 rpm at a measurement wavelength of 570 nm.**

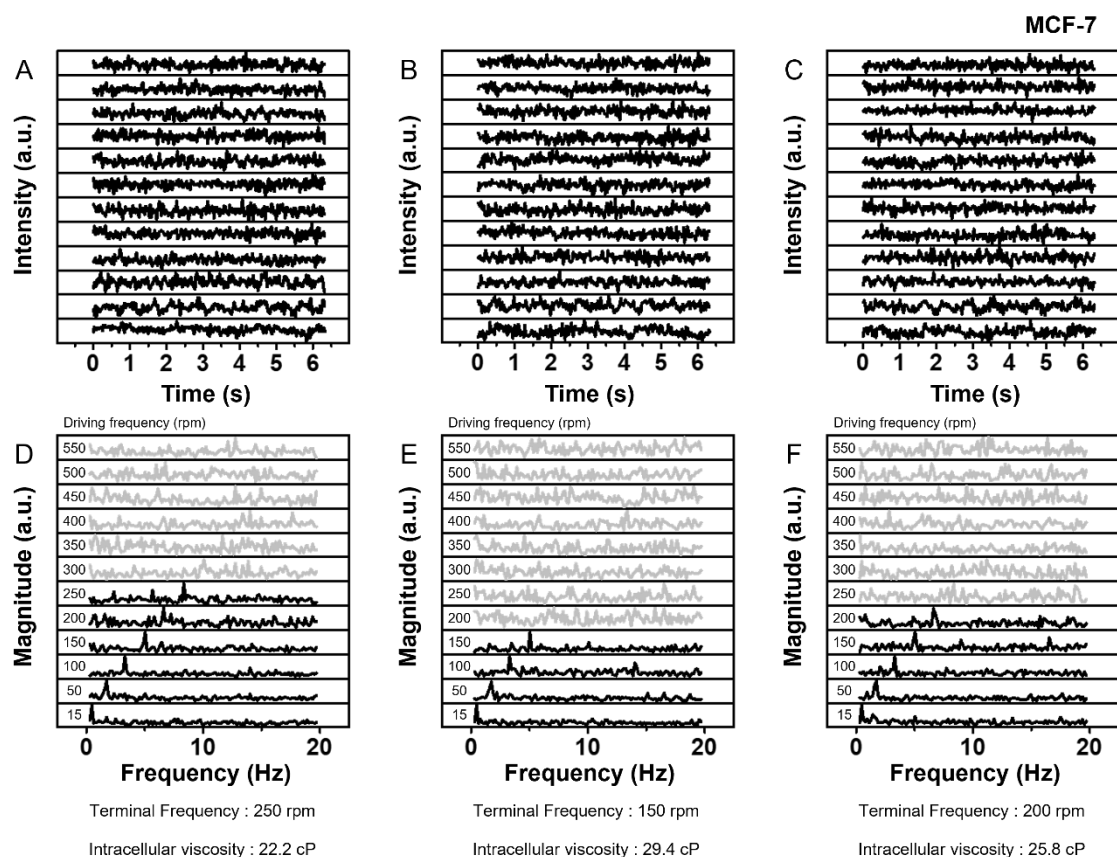


**Figure S38. Raw FTSPR data for viscosity measurement of MCF-7 cells (measurement 4, 5, and 6). (A-C) Raw optical response data and (D-F) their corresponding frequency peak data after FFT. Optical response data were obtained under driving frequencies from 15 rpm to 550 rpm at a measurement wavelength of 570 nm.**

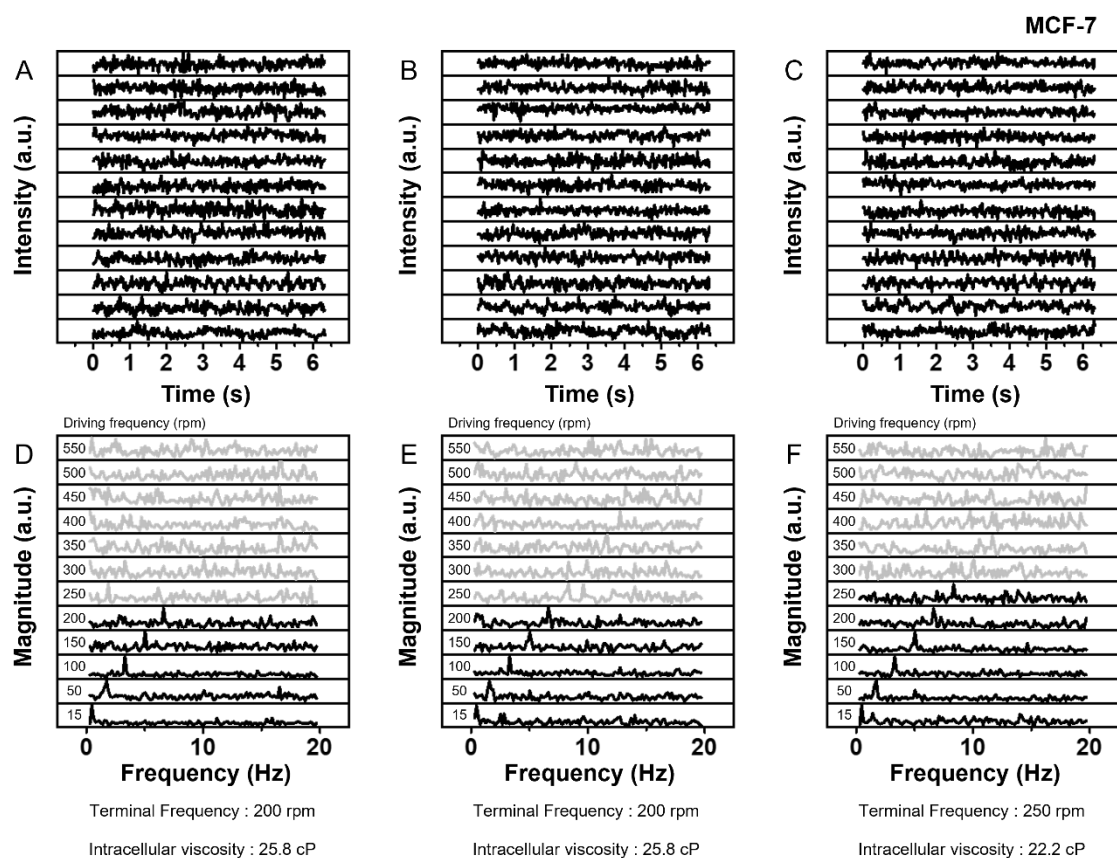
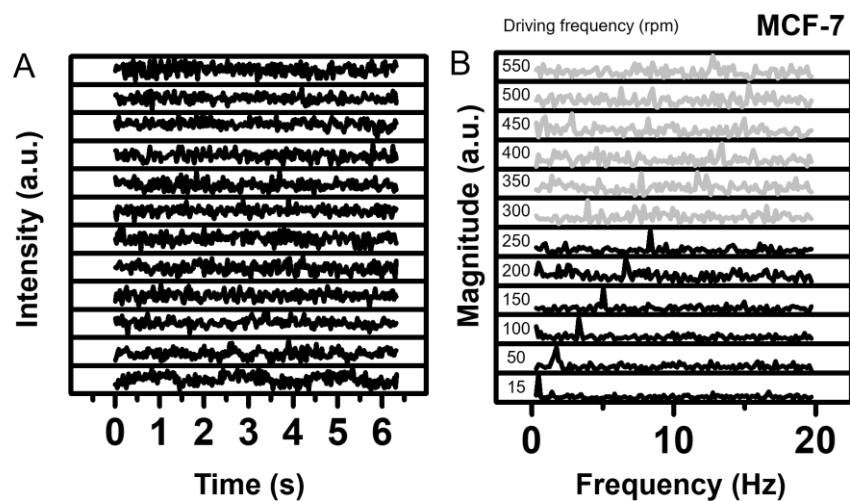


**Figure S39. Raw FTSPR data for viscosity measurement of MCF-7 cells (measurement 7, 8, and 9). (A-C) Raw optical response data and (D-F) their corresponding frequency peak data after FFT. Optical response data were obtained under driving frequencies from 15 rpm to 550 rpm at a measurement wavelength of 570 nm.**



Terminal Frequency : 250 rpm

Intracellular viscosity : 22.2 cP

**Figure S40. Raw FTSPR data for viscosity measurement of MCF-7 cells (measurement 10).**

(A) Raw optical response data and (B) their corresponding frequency peak data after FFT. Optical response data were obtained under driving frequencies from 15 rpm to 550 rpm at a measurement wavelength of 570 nm.

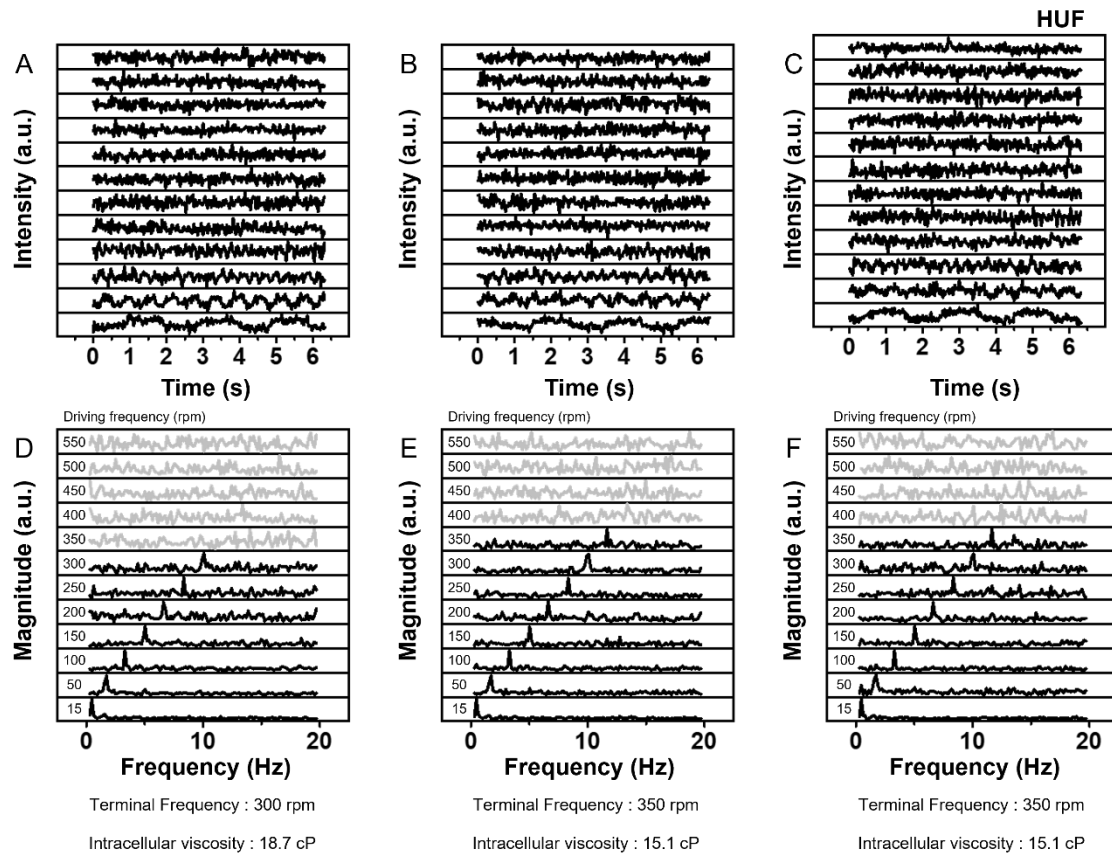


**Figure S41. Raw FTSPR data for viscosity measurement of HUF cells (measurement 1, 2, and 3). (A-C) Raw optical response data and (D-F) their corresponding frequency peak data after FFT. Optical response data were obtained under driving frequencies from 15 rpm to 550 rpm at a measurement wavelength of 570 nm.**

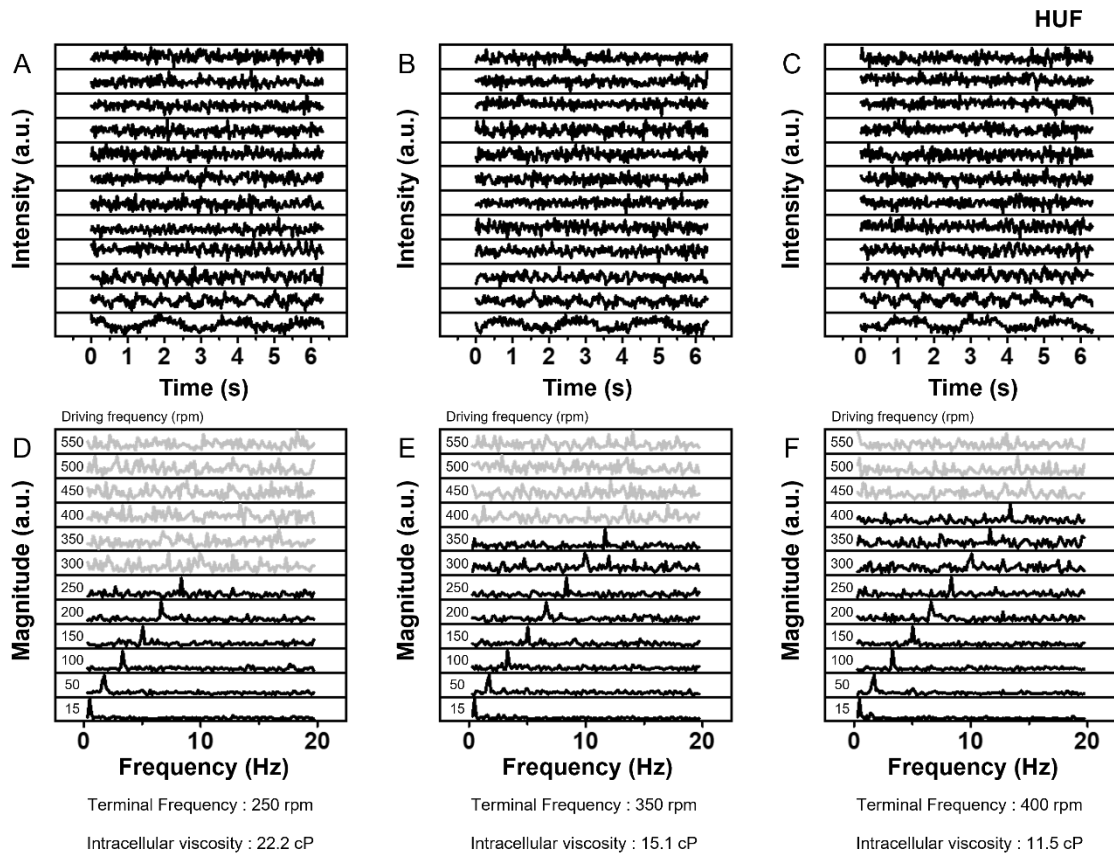


**Figure S42. Raw FTSPR data for viscosity measurement of HUF cells (measurement 4, 5, and 6). (A-C) Raw optical response data and (D-F) their corresponding frequency peak data after FFT. Optical response data were obtained under driving frequencies from 15 rpm to 550 rpm at a measurement wavelength of 570 nm.**

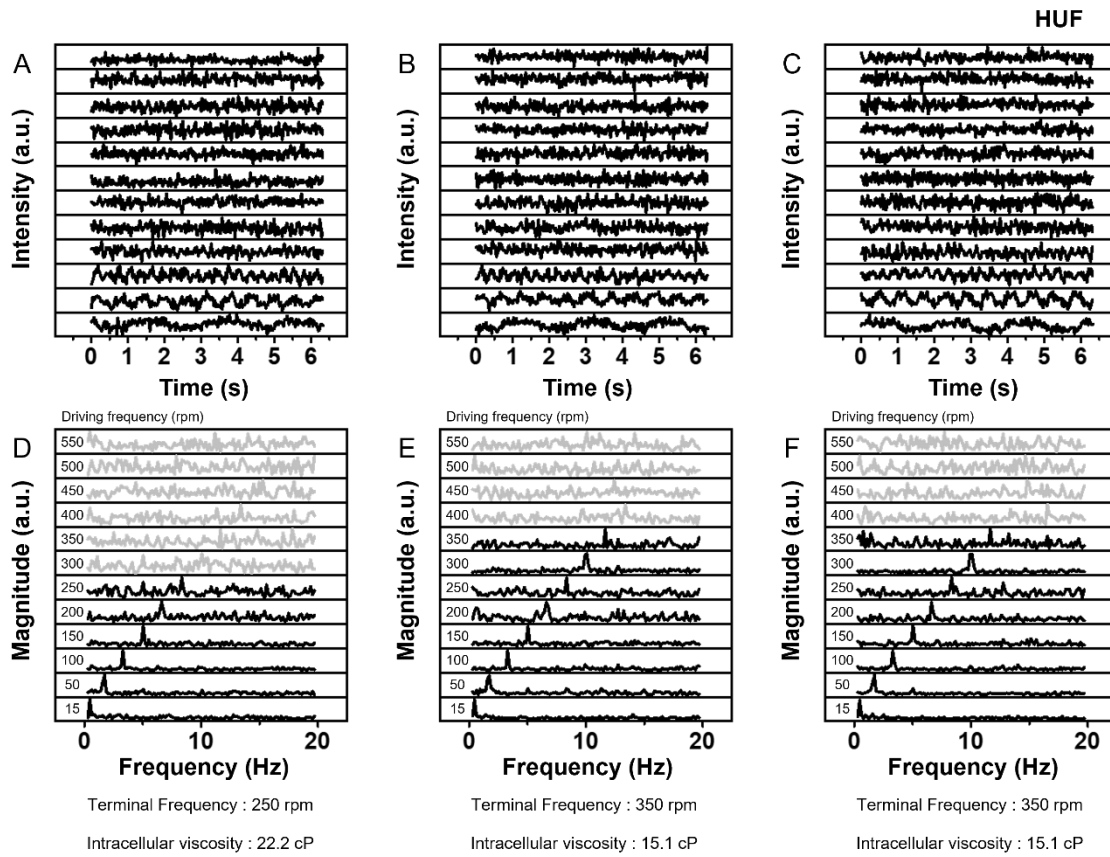
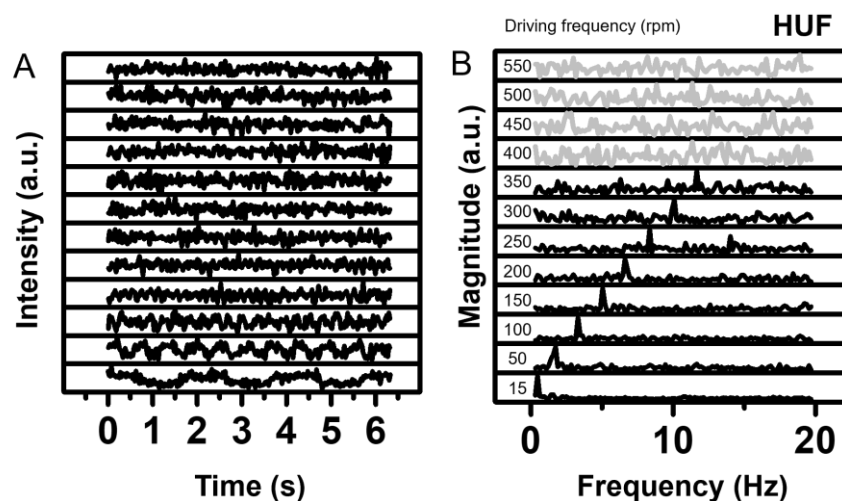


**Figure S43. Raw FTSPR data for viscosity measurement of HUF cells (measurement 7, 8, and 9). (A-C) Raw optical response data and (D-F) their corresponding frequency peak data after FFT. Optical response data were obtained under driving frequencies from 15 rpm to 550 rpm at a measurement wavelength of 570 nm.**





Terminal Frequency : 350 rpm

Intracellular viscosity : 15.1 cP

**Figure S44. Raw FTSPR data for viscosity measurement of HUF cells (measurement 10).** (A) Raw optical response data and (B) their corresponding frequency peak data after FFT. Optical response data were obtained under driving frequencies from 15 rpm to 550 rpm at a measurement wavelength of 570 nm.

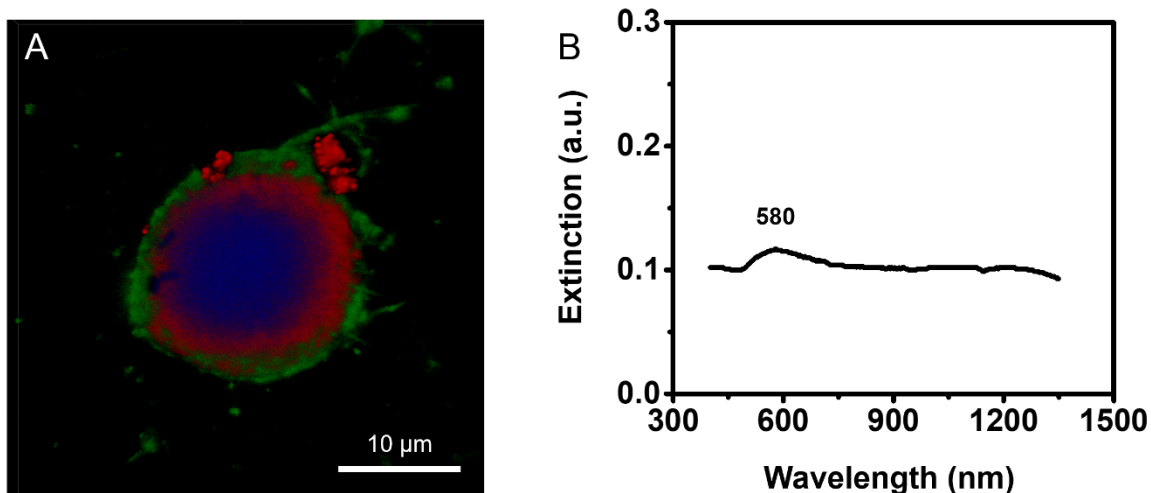


**Figure S45. Vis-NIR spectrum and CLSM image of Au/Ni/Au nanorods taken up by HeLa cells.** We obtained the CLSM image and vis-NIR spectrum of Au/Ni/Au nanorods taken up by HeLa cells. **(A)** When we added MUTAB modified Au/Ni/Au nanorods (concentration: 5 pM) to the cell (concentration: 5,000 cells / 100  $\mu\text{L}$ ) solution, MUTAB modified Au/Ni/Au nanorods were successfully localized in the cells in 30 minutes as shown in CLSM image. **(B)** From the vis-NIR spectrum measurement, the transverse mode of Au/Ni/Au nanorods (which has taken up by HeLa cells) was clearly shown at 580 nm. It is noteworthy that the longitudinal mode of NRs is a quadrupolar mode (not a dipole longitudinal mode) which shows weak intensity and easily becomes suppressed depending on the surrounding conditions.

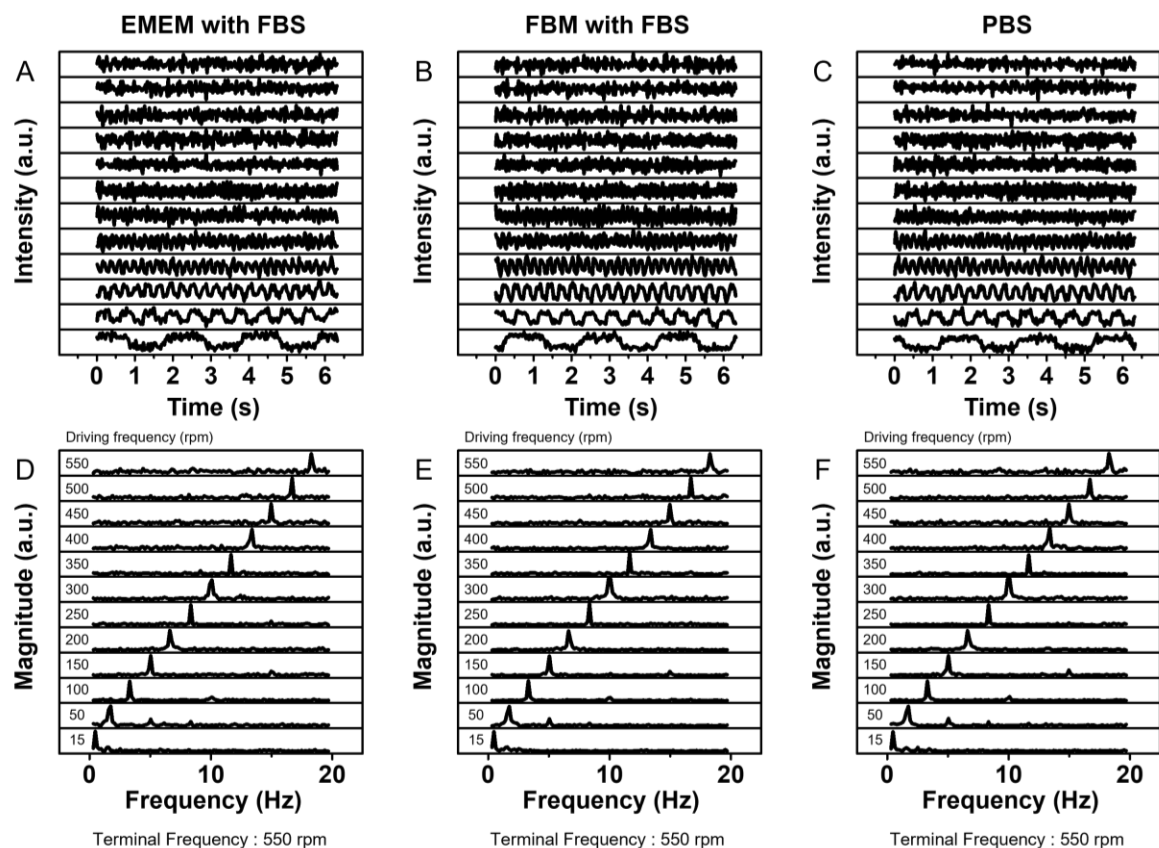


**Figure S46. Raw FTSPR data for viscosity measurement of cell culture medium and buffer solution.** Raw optical response data and their frequency peak data after FFT obtained from Au/Ni/Au nanorods dispersed in **(A, D)** EMEM with FBS, **(B, E)** FBM with FBS, and **(C, F)** PBS. Optical response data were obtained under driving frequencies from 15 rpm to 550 rpm at a measurement wavelength of 570 nm.

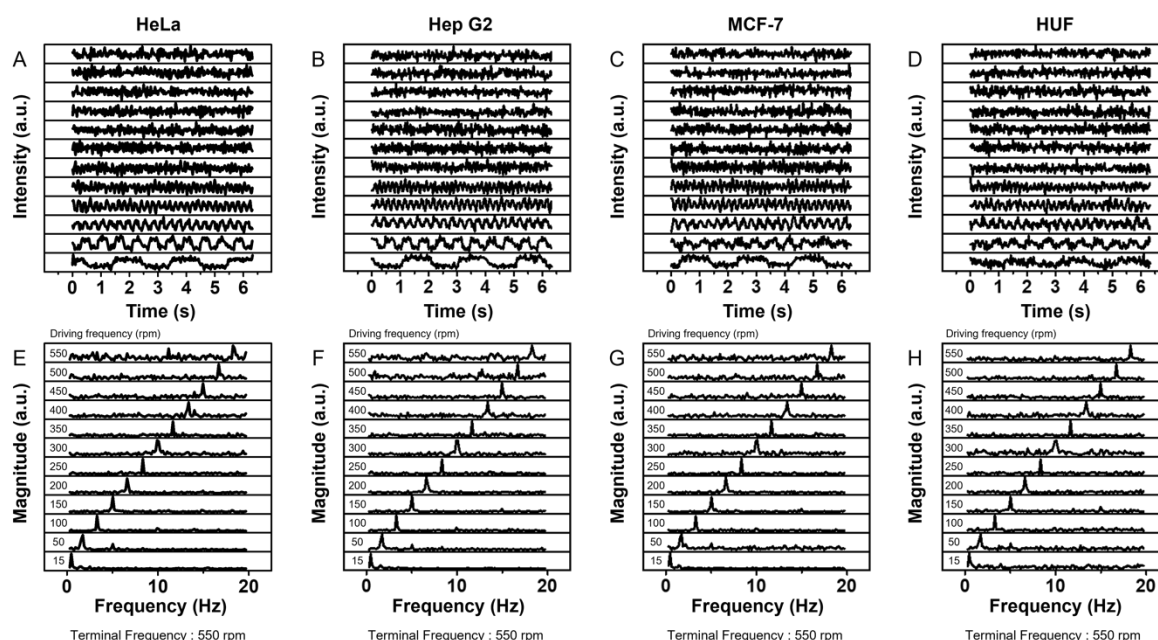


**Figure S47. Raw FTSPR data for viscosity measurement of HeLa, Hep G2, MCF-7, and HUF cells obtained immediately after adding Au/Ni/Au nanorods in the cell solution.** Raw optical response data and frequency peak data after FFT obtained from Au/Ni/Au nanorods immediately after adding Au/Ni/Au nanorods to the cell solution of **(A, E)** HeLa, **(B, F)** Hep G2, **(C, G)** MCF-7, and **(D, H)** HUF. Optical response data were obtained under a rotating magnetic field from 15 to 550 rpm at a measurement wavelength of 570 nm.

**Table S1. A comparison table of intracellular viscosity measurement**

Nanoprobe	Method	Viscosity range	Cell type	Ref
boron-dipyrin or BODIPY (4,4-difluoro-4-bora-3a,4a-diaza-s-indacene) based molecular rotors	Microviscosity by Fluorescent decay	$120 \pm 9$ cP	LDs in MCF-7 (human breast cancer cells)	[9]
		$195 \pm 48$ cP	MDA-MB-231 cells	
Porphyrin-dimer based rotor	Fluorescent lifetime-based ratiometric viscosity measurement	50 cP	Carcinoma of the Chinese hamster ovary (CHO) cell lines	[10]
meso-substituted 4,4'-difluoro-4-bora-3a,4adiazas-indacene	Fluorescent lifetime-based ratiometric viscosity measurement	80 cP	SK-OV-3 epithelial adenocarcinoma cell line	[11]
100-nm (diameter) carboxylated polystyrene beads	Video particle tracking	0.2-1 Pa·s	HeLa cells	[12]
2-6 $\mu$ m magnetic microwires	Rotational magnetic spectroscopy	30-80 Pa·s	NIH/3T3 fibroblasts	[13]
1-10 $\mu$ m magnetic microwires	Rotational magnetic spectroscopy	0.16 Pa·s	NIH/3T3 fibroblasts	[14]
HSA templated AuNCs (sizes of 1 to 4 nm)	Fluorescence correlation spectroscopy	~23 cP	HeLa cells	[15]
PET fluorescent probe	Fluorescence lifetime imaging	$130 \pm 20 \sim 175 \pm 20$ cP	Lysosomal regions in MCF-7 cells	[16]
		$60 \pm 20 \sim 120 \pm 20$ cP	Mitochondrial regions in MCF-7 cells	
8-hydroxyperene-1,3,6-trisulfonic acid (HPTS)	Time-dependent fluorescence anisotropy measurements	$1.00 \pm 0.03 \sim 2.21 \pm 0.05$ cP	J774 mouse macrophage cells	[17]

LDs: lipid droplets; HSA: Human Serum Albumin; PET: Photoinduced electron transfer

## References

- (1) Martin, C. R., Nanomaterials - a Membrane-Based Synthetic Approach. *Science* **1994**, *266*, 1961-1966.
- (2) Kim, S.; Shuford, K. L.; Bok, H. M.; Kim, S. K.; Park, S., Intraparticle surface plasmon coupling in quasi-one-dimensional nanostructures. *Nano. Lett.* **2008**, *8*, 800-804.
- (3) Jung, I.; Jang, H. J.; Han, S.; Acapulco, J. A. I.; Park, S., Magnetic Modulation of Surface Plasmon Resonance by Tailoring Magnetically Responsive Metallic Block in Multisegment Nanorods. *Chem. Mater.* **2015**, *27*, 8433-8441.
- (4) Jung, I.; Yoo, H.; Jang, H. J.; Cho, S.; Lee, K.; Hong, S.; Park, S., Fourier Transform Surface Plasmon Resonance (FTSPR) with Gyromagnetic Plasmonic Nanorods. *Angew. Chem. Int. Edit.* **2018**, *57*, 1841-1845.
- (5) Jung, I.; Ih, S.; Yoo, H.; Hong, S.; Park, S., Fourier Transform Surface Plasmon Resonance of Nanodisks Embedded in Magnetic Nanorods. *Nano. Lett.* **2018**, *18*, 1984-1992.
- (6) Hilal, H.; Lee, S.; Jung, I.; Yoo, S.; Park, S., Scattering Fourier Transform Biosensor: Binary Mixture Consisting of Magnetic Ni Nanorings and Plasmonic Au Nanorods. *Anal. Chem.* **2020**, *92*, 10099-10107.
- (7) J. B. Segur, H. E. Oberstar. Viscosity of glycerol and its aqueous solutions. *Ind. Eng. Chem.* **1951**, *43*, 2117-2120.
- (8) Klyushin, A. Y.; Rocha, T. C. R.; Havecker, M.; Knop-Gericke, A.; Schlogl, R. A near ambient pressure XPS study of Au oxidation. *Phys. Chem. Chem. Phys.* **2014**, *16*, 7881-7886.
- (9) Jurgutis, D.; Jarockyte, G.; Poderys, V.; Dodonova-Vaitkuniene, J.; Tumkevicius, S.; Vysniauskas, A.; Rotomskis, R.; Karabanovas, V. Exploring BODIPY-Based Sensor for Imaging of Intracellular Microviscosity in Human Breast Cancer Cells. *Int. J Mol. Sci.* **2022**, *23*, 5687.
- (10) Kuimova, M. K.; Botchway, S. W.; Parker, A. W.; Balaz, M.; Collins, H. A.; Anderson, H. L.; Suhling, K.; Ogilby, P. R. Imaging intracellular viscosity of a single cell during photoinduced cell death. *Nat. Chem.* **2009**, *1*, 69-73.
- (11) Kuimova, M. K.; Yahioğlu, G.; Levitt, J. A.; Suhling, K. Molecular rotor measures viscosity of live cells via fluorescence lifetime imaging. *J. Am. Chem. Soc.* **2008**, *130*, 6672-6673.
- (12) Chen, Y. Q.; Kuo, C. Y.; Wei, M. T.; Wu, K.; Su, P. T.; Huang, C. S.; Chiou, A. Intracellular viscoelasticity of HeLa cells during cell division studied by video particle-tracking microrheology.

*J. Biomed. Opt.* **2014**, *19*, 011008.

(13) Berret, J. F. Local viscoelasticity of living cells measured by rotational magnetic spectroscopy. *Nat. Commun.* **2016**, *7*, 10134.

(14) Chevry, L.; Colin, R.; Abou, B.; Berret, J. F. Intracellular micro-rheology probed by micron-sized wires. *Biomaterials* **2013**, *34*, 6299-6305.

(15) Chakraborty, S.; Nandi, S.; Bhattacharyya, K.; Mukherjee, S. Probing Viscosity of Co-Polymer Hydrogel and HeLa Cell Using Fluorescent Gold Nanoclusters: Fluorescence Correlation Spectroscopy and Anisotropy Decay. *Chemphyschem* **2020**, *21*, 406-414.

(16) Liu, T.; Liu, X.; Spring, D. R.; Qian, X.; Cui, J.; Xu, Z. Quantitatively mapping cellular viscosity with detailed organelle information via a designed PET fluorescent probe. *Sci. Rep.* **2014**, *4*, 5418.

(17) Parker, W. C.; Chakraborty, N.; Vrikkis, R.; Elliott, G.; Smith, S.; Moyer, P. J. High-resolution intracellular viscosity measurement using time-dependent fluorescence anisotropy. *Opt. Express.* **2010**, *18*, 16607-16617.